Mon. Not. R. Astron. Soc. **264,** 455–488 (1993)

# Infrared imaging of the host galaxies of radio-loud and radio-quiet quasars

J. S. Dunlop,[1,2] G. L. Taylor,[2] D. H. Hughes[2]★ and E. I. Robson[2]

[1] *Chemical and Physical Sciences, Liverpool John Moores University, Byrom Street, Liverpool L3 3AF*
[2] *Department of Physics and Astronomy, University of Central Lancashire, Preston PR1 2HE*

Accepted 1993 March 18. Received 1993 March 8; in original form 1992 July 27

**ABSTRACT**

We present initial results from the first deep near-infrared imaging study of the host galaxies of an extensive sample of low-redshift ($z < 0.4$) radio-loud and radio-quiet quasars. To minimize selection effects, the radio-loud and radio-quiet subsamples have been selected to be indistinguishable in terms of their distributions on the $V$–$z$ plane, and classification as radio-loud or radio-quiet is defined in terms of 5-GHz luminosity.

We discuss the problems associated with accurate determination of the infrared point spread function (PSF) and our adopted solution of an a posteriori selection from a 'library' of observationally determined PSFs. Images reaching surface brightness levels of $\mu_K = 22$ mag arcsec$^{-2}$ of the quasar hosts, before and after subtraction of the nuclear component, are then presented.

After removal of the nuclear component, the host galaxies of both classes of quasar are found to be good 'standard candles' at $K$, displaying a $K$–$z$ relation essentially identical to that already established for radio galaxies. In addition, we find no evidence that radio-loud and radio-quiet hosts differ in terms of $K$-band luminosity; both appear to be selected solely from the top of the $K$-band galaxy luminosity function.

We briefly compare the dimensions and near-infrared morphologies of the radio-loud and radio-quiet hosts and, in the case of radio-loud quasars, investigate the relationship between near-infrared and radio morphology. Finally, we give a preliminary discussion of the significance of the universal incidence of apparent companion objects in our images.

A detailed analysis of the luminosity profiles and companion statistics derived from the images presented here will be the subject of subsequent papers.

**Key words:** galaxies: active – galaxies: photometry – quasars: general – infrared: galaxies.

## 1 INTRODUCTION

The relationship between radio-loud and radio-quiet quasars (hereafter RLQs and RQQs respectively) is one of the most fundamental, long-standing and controversial issues in active-galaxy research. An understanding of both the differences and similarities between these two classes of source is of central importance in any attempt to unify or relate the various manifestations of the AGN phenomenon.

★ Present address: Astrophysics, Department of Physics, University of Oxford, Keble Road, Oxford OX1 3RH.

This problem can be tackled from various angles, each of which undoubtedly has an important contribution to make. One approach is to focus on the wavelength regime in which the spectra of RQQs and RLQs are most strongly divergent, in particular to establish the nature of the far-infrared to sub-millimetre emission from RQQs (Chini, Kreysa & Biermann 1989; de Kool & Begelman 1989; Schlickheiser, Biermann & Crusius-Wätzel 1991; Hughes et al. 1993). A second approach is to investigate the form of the quasar radio luminosity function (Peacock, Miller & Longair 1986; Miller, Peacock & Mead 1990). Further sources of valuable input include polarization studies (Berriman et al. 1990; Sitko &

Zhu 1991), modelling of the detailed form of the infrared-to-ultraviolet continuum (e.g. Barvainis 1990), comparison of the cosmological evolution of RLQs and RQQs (Dunlop & Peacock 1990), and investigation of correlations between emission from different regions of the spectrum (e.g. the far-IR–radio correlation; Sopp & Alexander 1991).

Nevertheless, it has become increasingly clear that one of the key pieces in the jigsaw is likely to be provided by studies of the environments of quasars. The term 'environment' covers a wide range of scales, from the ~0.5 Mpc clustering environments investigated by Ellingson, Yee & Green (1991), to the distribution of emission-line regions within a few kiloparsec of the central nucleus, but it is at intermediate scales that most attention has been directed, in the attempt to determine the nature and immediate environment of the host galaxies of quasars. By technical necessity, virtually all previous studies of quasar hosts have been carried out at optical wavelengths. In this paper we present results from the first extensive infrared imaging study of the host galaxies of radio-loud and radio-quiet quasars.

Since optical 'fuzz' was first observed around quasars (Kristian 1973), numerous imaging and off-nuclear spectroscopic studies of quasars with $z < 0.5$ have shown that the properties of this fuzz are indeed consistent with those of large galaxies at the relevant redshifts (e.g. Boroson, Oke & Green 1982; Boroson & Oke 1984; Gehren et al. 1984; Hutchings, Crampton & Campbell 1984a; Malkan, Margon & Chanan 1984; Boroson, Persson & Oke 1985; Smith et al. 1986; Hutchings, Janson & Neff 1989; Romanishin & Hintzen 1989). Many of these studies have attempted comparison of the hosts of RLQs and RQQs, in an attempt to verify or refute the widely held belief that RLQs lie in giant elliptical galaxies, while RQQs reside in spirals. This belief is largely motivated by the 'fact' that all powerful radio *galaxies* are ellipticals, whereas low-redshift Seyferts (which are known to be very weak radio-emitters in comparison to radio-selected quasars; Meurs & Wilson 1984) have spiral hosts (MacKenty 1990). This idea, coupled with the apparent success of schemes involving the unification of powerful radio galaxies and quasars via orientation effects (e.g. Barthel 1989), has led naturally to associated studies comparing the properties of RLQ hosts with those of radio galaxies (Hutchings 1987; Smith & Heckman 1990).

In many respects the results of these various studies appear to be in qualitative (although rarely quantitative) agreement, but the situation is still confused. For example, one consistent finding is that the host galaxies of RLQs are (on average) brighter than the hosts of RQQs, suggesting that RLQs do indeed lie in massive ellipticals. However, the claimed size of this systematic difference varies from 2 mag (Gehren et al. 1984) to 0.7 or 0.8 mag (Smith et al. 1986). Hutchings et al. (1989) find the average magnitude difference to be 1.3 in $R$, rising to 1.9 in $B$, a wavelength dependence consistent with previous claims that RLQ hosts have bluer $B-V$ colours than their RQQ counterparts (Hickson & Hutchings 1987). This latter result confuses the situation somewhat, since elliptical galaxies would normally be expected to display redder optical colours than disc galaxies.

In addition to determining the magnitudes and colours of the host galaxies, some authors (e.g. Smith et al. 1986) have attempted detailed modelling of their luminosity profiles. The results of these analyses have been broadly consistent with the idea that RQQs lie in discs, whereas the hosts of RLQs are better described by a de Vaucouleurs $r^{1/4}$ luminosity profile. With a few exceptions, however, unambiguous discrimination has proved difficult.

In considering these results, it is important to note the dangerous impact of selection effects. With the exception of Hutchings et al. (1989), all of the above-mentioned studies suffer from poor sample control. Several of the RQQs included in the samples actually have luminosities fainter than the 'accepted' dividing line between Seyferts and quasars at $M_V = -23.0$ (Véron-Cetty & Véron 1991). It is therefore inevitable that the hosts of these low-power RQQs should have properties similar to those of Seyferts. The quasar–Seyfert division is, of course, a somewhat subjective one, but the important point is the lack of RLQs of comparable absolute magnitude and redshift. Even when sample selection is confined to quasars brighter than $M_V = -23.0$, the relative rarity of RLQs means that care must still be exerted to ensure that the redshift and luminosity distributions of the two comparison samples are well matched.

The importance of well-matched samples was fully appreciated in the most recent extensive optical study of quasar hosts by Véron-Cetty & Woltjer (1990), and so it is interesting that some of their conclusions differ significantly from those of the earlier studies described above. They obtained $i$-band images of 20 RLQs and 16 RQQs in the luminosity band $-24.6 > M_V > -26.6$, and concluded in favour of a picture in which elliptical galaxies provide the hosts of RLQs and also a 'substantial part' of the RQQ population. This conclusion was based mainly on magnitude and colour data, since they found that most of their host-galaxy images could be fitted equally well by spheroidal or disc models. They also concluded that RLQ hosts and radio galaxies have the same $\langle M_V \rangle$ and the same dispersion, a result in direct contradiction to that of Hutchings (1987), who concluded that radio galaxies and RLQ hosts are not, in fact, the same type of object. Finally, it is interesting to note that, although Véron-Cetty & Woltjer confirm earlier findings that RQQ hosts are on average fainter than their RLQ counterparts, they find the size of this systematic magnitude difference to be as small as $\Delta i \simeq 0.6$ mag.

That the nature of RLQ and RQQ hosts should remain unresolved after a decade of extensive study is largely a reflection of the fact that the optical is not the ideal waveband in which to investigate the problem. First, there is growing evidence that AGN are associated with or could even stimulate star formation activity which, in the optical–UV, could mask the true nature of the underlying galaxy (e.g. McCarthy et al. 1987). Secondly, by definition, quasars are heavily nuclear-dominated objects in the optical, making galaxy magnitude determination and profile analysis extremely sensitive to the estimated strength of the core component. Thirdly, optical filters are susceptible to contamination by strong emission lines. These problems were recognized by Véron-Cetty & Woltjer in their choice of the $i$-band filter, but it is clear that the problem can be better addressed by moving to still longer wavelengths; the spectrum of an elliptical galaxy peaks at $\simeq 1.6$ μm, making $K$ (2.2 μm) the optimum waveband for detection of elliptical hosts at redshifts $z \simeq 0.2$–$0.3$.

In an attempt to exploit these perceived advantages of the near-infrared, we have carried out an extensive deep $K$-band imaging study of a sample of 32 quasars. Because of the lack

of imaging devices, previous near-infrared studies have been confined to multi-aperture photometry using an occulting disc (Neugebauer et al. 1985), allowing only a crude, seeing-dependent analysis of the magnitudes and colours of the host galaxies.

In this paper we describe the properties of the quasar sample, the observing technique, and the problems involved in accurate subtraction of the point spread function (PSF). We then present the *K*-band images of the quasars before and after removal of the nuclear component, and discuss the implications of the *K* magnitudes of the host galaxies. Finally, we give a brief preliminary discussion of the basic morphologies of the host galaxies, and the significance of the apparently high incidence of companion objects. A detailed analysis of the luminosity profiles of the hosts and of the statistics of companion objects will be presented in subsequent papers. $H_0 = 50$ km s$^{-1}$ Mpc$^{-1}$ and $\Omega_0 = 1$ are assumed throughout.

## 2 DATA

### 2.1 Observations

The infrared images were taken with the $62 \times 58$ pixel$^2$ InSb array camera IRCAM (McLean et al. 1986) on the 3.9-m United Kingdom Infrared Telescope (UKIRT), with the camera operating in the 0.62 arcsec pixel$^{-1}$ mode. *K*-band images were obtained from four successive observing runs between 1989 October and 1991 March.

Each quasar was imaged using an identical procedure which was designed to ensure highly accurate flat-fielding. Integrations were subdivided into 17 individual 3-min exposures (which were themselves divided into coadds of integration whose duration was chosen to avoid saturation of the quasar nucleus). The odd-numbered frames were all centred on the quasar position, providing a total of 27 min of on-source integration. The intervening even-numbered frames were used to obtain 3-min images of eight different regions of sky around the quasar ($\simeq 1$ arcmin off-source). These eight sky frames were then median-filtered to produce an accurate sky flat-field concurrent with the observation.

The basic reduction procedure was as follows: (i) subtraction of a dark + bias frame from each 3-min subimage; (ii) interpolation over known bad pixels and trimming of faulty rows at the top of the array; (iii) correction of frame-to-frame DC variations followed by median-filtering through the eight sky-frame stack; (iv) normalization of the resulting flat-field; (v) flat-fielding of each of the nine on-source images; (vi) construction of the final image from the average of the nine flat-fielded on-source images (after checking for accurate registration).

The resulting images consist of only 27 min of on-source integration from a total observation time of $\simeq 1$ h, but experimentation showed that this apparently extravagant procedure was justified by the depth of the final images made possible by the accuracy of flat-fielding (since the quasar hosts generally occupy a considerable fraction of the small IRCAM field of view, it was not possible to produce a median-filtered flat by simply shifting the position of the source within the bounds of the detector).

For all but one very low-redshift quasar (2130+099; $z = 0.061$), two separate 27-min images were obtained. These were then compared to allow cosmic ray events to be identified and removed, before being registered and averaged to produce the final 54-min image. Finally, the completed images were smoothed with a Gaussian filter of width $\sigma = 0.7$ pixel.

To calibrate the photometry (and to provide high signal-to-noise samples of the PSF; see Section 3.1), photometric standards in the same fields as the target objects were observed regularly throughout each night of observation. Flat-fielding of these star images was adequately achieved by simple subtraction of a sky-frame of equivalent integration time.

### 2.2 Sample properties

#### 2.2.1 V–z *distributions*

The principal objective of the initial two-night observing run in 1989 October was to explore the feasibility of imaging quasar hosts in the infrared. For this reason our first 'trial' sample of six quasars contained examples of very low-redshift RQQs such as 2130+099. In subsequent observing runs, however, target selection was dictated (as far as possible) by the aim of achieving final samples of RQQs and RLQs whose distributions in the *V*–*z* plane were well matched (Hutchings et al. 1989). In addition, we decided to limit the redshift range of the sample to $0.08 < z < 0.35$, since the IRCAM field of view is ideally suited to the imaging of large galaxies within this redshift range; beyond $z \simeq 0.4$, detection of quasar hosts is extremely difficult, given the IRCAM PSF.

The final quasar sample containing 14 RLQs and 18 RQQs (classified as described below) is listed in Table 1. The four brightest RQQs with $V \leq 15$ (1211+143, 1216−015, 1440+356 and 2130+099) clearly have no RLQ counterparts, and have therefore been excluded from any subsequent comparison of the two samples. The *V*–*z* distributions of the resulting 'matched' samples of 14 RLQs and 14 RQQs are shown in Fig. 1. Comparison of these two distributions via the two-dimensional Kolmogorov–Smirnov (KS) test (Peacock 1983) shows that, in terms of these two observed parameters, the two samples are statistically indistinguishable (significance level $p = 0.13$, whereas prior to removal of the four bright RQQs, $p = 0.03$).

#### 2.2.2 *Radio-loud and radio-quiet classification*

Our classification of a quasar as radio-loud or radio-quiet is based on radio power rather than, for example, the ratio of radio to optical luminosity *R* (Schmidt 1970). From a study of the radio properties of a sample of optically selected quasars in the narrow redshift band $1.8 < z < 2.5$, Miller et al. (1990) found strong evidence of bimodality in the quasar radio luminosity function. In particular, their large number of non-detections indicates the presence of a gap in the quasar luminosity function extending from $L_{5\,\mathrm{GHz}} \simeq 10^{25}$ W Hz$^{-1}$ sr$^{-1}$ down to at least $L_{5\,\mathrm{GHz}} \simeq 10^{24}$ W Hz$^{-1}$ sr$^{-1}$ (the effective detection limit of their survey). This result is, in fact, one of the strongest pieces of evidence that there exist two distinct quasar populations. In addition, they found no evidence for any correlation between the radio and optical luminosities of the radio-loud quasars, indicating the irrelevance of the parameter *R*, at least for the radio-loud population. In Fig. 2, we plot the distribution of radio and optical luminosities of the quasars in our $z < 0.4$ sample for which radio

**Table 1.** The quasar sample. Redshifts $z$, radio fluxes $S_{5\,\mathrm{GHz}}$, radio spectral indices $\alpha$ ($f_\nu \propto \nu^{-\alpha}$), and apparent and absolute magnitudes $V$ and $M_V$ have been taken from table 1 of Véron-Cetty & Véron (1991). Classification as radio-loud or radio-quiet is based on 5-GHz luminosity (see Section 2.2.2).

| Classification | Name | $z$ | $S_{5GHz}$ (Jy) | $\alpha_{2.7GHz}$ | $V$ | $M_V$ |
|---|---|---|---|---|---|---|
| **Radio Loud** | 0137+012 | 0.258 | 0.830 | 0.37 | 17.07 | −23.9 |
| | 0204+292 | 0.109 | 0.840 | 0.76 | 16.00 | −23.0 |
| | 0736+017 | 0.191 | 1.920 | 0.10 | 16.47 | −23.8 |
| | 1004+130 | 0.240 | 0.420 | 0.68 | 15.15 | −25.7 |
| | 1020−103 | 0.197 | 0.390 | 0.62 | 16.11 | −24.2 |
| | 1048−090 | 0.345 | 0.680 | 0.92 | 16.97 | −24.9 |
| | 1217+023 | 0.240 | 0.470 | −0.03 | 16.53 | −24.3 |
| | 1223+252 | 0.268 | 0.127 | 0.70 | 17.12 | −24.0 |
| | 2135−147 | 0.200 | 1.310 | 0.75 | 15.53 | −24.9 |
| | 2141+175 | 0.213 | 0.500 | −0.49 | 15.73 | −24.8 |
| | 2201+315 | 0.298 | 2.310 | −0.27 | 15.58 | −25.8 |
| | 2247+140 | 0.237 | 1.030 | 0.62 | 16.93 | −23.9 |
| | 2349−014 | 0.173 | 0.700 | 0.59 | 15.33 | −24.7 |
| | 2355−082 | 0.211 | 0.220 | 0.21 | 17.50 | −23.0 |
| **Radio Quiet** | 0007+106 | 0.090 | 0.321 | −0.98 | 15.40 | − 23.3 |
| | 0046+112 | 0.275 | <0.043 | | 17.10 | −24.1 |
| | 0052+251 | 0.154 | 0.00074 | | 15.90 | −23.9 |
| | 0054+144 | 0.171 | <0.025 | | 15.71 | −24.3 |
| | 0157+001 | 0.163 | 0.008 | | 15.69 | −24.2 |
| | 0244+194 | 0.176 | <0.025 | | 16.66 | −23.4 |
| | 0257+024 | 0.115 | <0.025 | | 16.10 | −23.0 |
| | 0923+201 | 0.190 | 0.00025 | | 15.83 | −24.4 |
| | 0953+414 | 0.239 | 0.0019 | | 15.55 | −25.3 |
| | 1012+008 | 0.185 | 0.001 | | 15.85 | −24.3 |
| | 1211+143 | 0.085 | 0.157 | | 14.63 | −23.9 |
| | 1216−015 | 0.103 | <0.25 | | 15.00 | −23.9 |
| | 1440+356 | 0.079 | 0.00166 | | 14.58 | −23.8 |
| | 1549+203 | 0.250 | <0.025 | | 16.50 | −24.4 |
| | 1635+119 | 0.146 | 0.080 | 0.52 | 16.50 | −23.1 |
| | 2130+099 | 0.063 | 0.00205 | | 14.64 | −23.3 |
| | 2215−037 | 0.241 | <0.25 | | 17.20 | −23.7 |
| | 2344+184 | 0.138 | <0.025 | | 15.90 | −23.6 |

fluxes are available in the literature. Also included for comparison are the data on the high-redshift sample of Miller et al. (1990). From this diagram it is clear that our sample displays a similar distinct gap in radio luminosity (although it should be noted that, unlike the high-redshift sample, our low-redshift sample is in no sense complete). In general, because of this apparent gap, classification of the quasars in the sample is fairly clear-cut, but, for the sake of definiteness, we have classified as radio-quiet any quasar whose radio luminosity lies below $L_{5\,\mathrm{GHz}} \simeq 10^{24}$ W Hz$^{-1}$ sr$^{-1}$. For only three quasars does the classification depend crucially on the exact choice of critical luminosity; 0007+016, 1211+143 and 1635+119 are classified as radio-quiet by our criterion, despite their relatively bright observed radio fluxes $S_{5\,\mathrm{GHz}} > 50$ mJy (although there is evidence that the radio flux of 1211+143 was overestimated by Kellermann et al. 1989; Miller & Rawlings, private communication). We have also

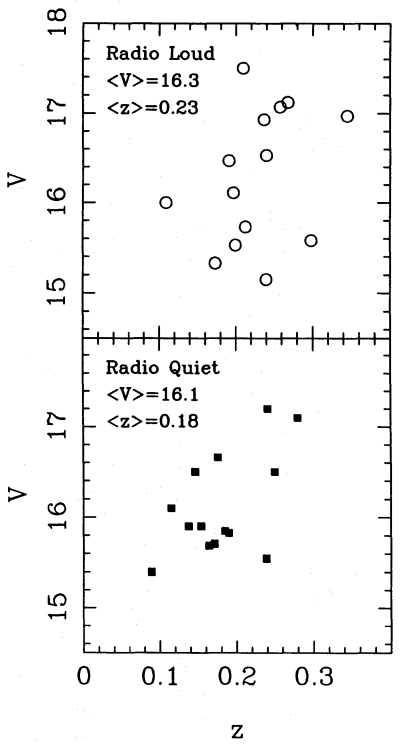


**Figure 1.** Distributions on the $V$–$z$ plane of the RLQ and RQQ samples after removal of the four RQQs with $V \leq 15$ (1211+143, 1216−015, 1440+356 and 2130+099). Prior to removal of these four bright RQQs, comparison of the two samples via the two-dimensional Kolmogorov–Smirnov test (Peacock 1983) yields a significance level of $p = 0.03$, whereas afterwards the two samples of 14 objects are statistically indistinguishable ($p = 0.13$).

classified as radio-quiet the eight quasars in the sample for which no measured radio fluxes exist since, for all but one of these sources, their non-detection in existing radio surveys (e.g. Bennett et al. 1986; Gregory & Condon 1991) constrains their radio luminosities to lie below the $L_{5\,\mathrm{GHz}} \simeq 10^{24}$ W Hz$^{-1}$ sr$^{-1}$ limit (upper limits shown as arrows in Fig. 2). Only for 2215−037 have we had simply to assume that its radio luminosity lies below this threshold.

Finally, Fig. 2 also serves to emphasize further the similar range of optical luminosities spanned by our RLQ and RQQ samples, and the fact that no quasar in either sample has $M_V > -23.0$.

## 3 IMAGE ANALYSIS

### 3.1 Determination of the point spread function

The extent to which the properties of quasar host galaxies can be accurately determined is crucially dependent on accurate removal of the nuclear contribution. The precise amount of nuclear luminosity that should be attributed to the quasar rather than to the galaxy is a model-dependent quantity, but of more fundamental importance is the accuracy with which the form of the PSF can be determined for each image. In optical CCD studies this problem is often fairly trivial because the relatively large field of view frequently contains bright stars which provide direct samples of

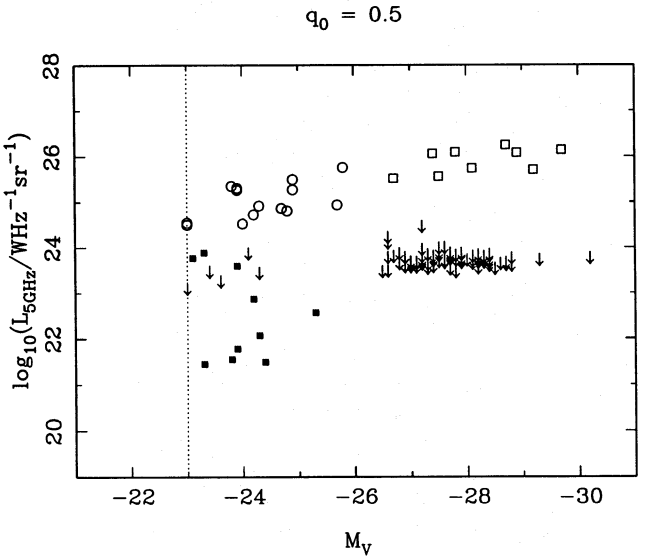


**Figure 2.** Radio luminosity at 5 GHz plotted against optical luminosity ($M_V$) for the $1.8 < z < 2.5$ quasar sample of Miller et al. (1990) and for those sources in the present $z < 0.4$ quasar sample for which radio fluxes are available in the literature (24 out of 32). Radio detections from Miller et al. are shown as open squares, with the upper limits implied by their non-detections being indicated by arrows. The choice of symbols for our low-redshift sample reflects the adoption of $L_{5\,GHz} = 10^{24}$ W Hz$^{-1}$ sr$^{-1}$ as the dividing line between RLQs (open circles) and RQQs (filled squares), but the diagram emphasizes that for virtually all objects the classification is extremely clear-cut due to the apparent gap in the radio luminosity function. Upper limits on the radio power of five RQQs in the low-redshift sample are also indicated by arrows (Bennett et al. 1986; Gregory & Condon 1991). The dotted line at $M_V = -23.0$ indicates the 'accepted' optical luminosity division between quasars and Seyfert galaxies. $H_0 = 50$ km s$^{-1}$ Mpc$^{-1}$ and $\Omega_0 = 1$ have been assumed.

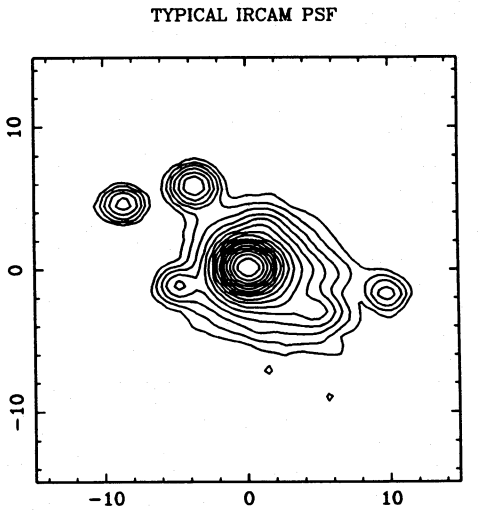


**Figure 3.** Example of a *K*-band IRCAM stellar image, showing the complex pattern of ghost images in the point spread function. Contours are a factor of 1.585 apart in flux, for direct comparison with the 0.5-mag contour intervals employed in Figs 4, 5 and 6.

the PSF for the exposure in question (e.g. Gehren et al. 1984). Unfortunately, the small IRCAM field of view ($38 \times 36$ arcsec$^2$) meant that this was hardly ever the case in the present study. The problem was further exacerbated by the rather crude sampling provided by the 0.62-arcsec pixel-scale, and also by the complex two-dimensional structure which the IRCAM PSF was found to possess (Fig. 3); this essentially precludes simple theoretical representations of the PSF (such as a double Gaussian; Smith et al. 1986).

The solution adopted was to exploit the observations of photometric standards to assemble a 'library' of ~100 high signal-to-noise PSFs, from which the PSF relevant to each quasar image could be selected a posteriori. This involved taking considerably deeper exposures of standards than was required simply for accurate photometric calibration. A separate library of PSFs had to be assembled for each observing run because the two-dimensional structure (largely due to ghosting) was found to vary from run to run.

The procedure used to select the correct PSF for each quasar image was as follows. First, to minimize sampling differences, the quasar image and all the star images taken during the relevant observing run were mapped on to new arrays such that their centroids were coincident with the centre of the central pixel. Next, after background subtraction, all stars in the PSF library were scaled to the same central pixel value as the quasar. The upper portion of the quasar image (i.e. all pixels with values higher than 40 per cent of the central pixel value) was then compared with the corresponding portion of every stellar image using the $\chi^2$ statistic. The five stars that yielded the lowest $\chi^2$ values were then selected as the best representations of the PSF for the quasar image in question; identification of an ensemble of candidate PSFs enables the sensitivity of subsequent analysis to the exact choice of PSF to be investigated.

### 3.2 Removal of ghosts

In addition to achieving accurate subtraction of the central PSF, it was important for all the ghost images associated with the bright central peak to be removed, particularly since these ghosts often bear a frightening resemblance to genuine compact companion objects. Unfortunately, although always occurring in roughly the same regions of the frame (during a given observing run), the exact positions of the ghosts relative to the central source were found to be a sensitive function of the position of the source on the array. As a consequence, subtraction of the minimum-$\chi^2$ stars hardly ever led to the desirable simultaneous removal of the central peak *and* its attendant ghosts, since the probability that even one of the five stars selected as a good representation of the PSF was also centred on exactly the same pixel coordinate as the quasar (in the raw frame) was extremely small. Therefore, prior to subtraction, the ghosts on both star and quasar images were simply 'patched' over by linear interpolation; ghosts in the quasar image were distinguished from genuine companion sources by comparison with the image of a star that had been imaged at exactly the same pixel coordinate as the quasar (but whose PSF in general made it unsuitable for removal of the central peak).

### 3.3 Removal of the nuclear contribution

In producing the images of the host galaxies we have adopted the model-independent approach of simply subtracting the

PSF scaled to the same height as the central peak of the quasar (i.e. the value of the central pixel in the residual host galaxy image is zero). The nuclear component has therefore been deliberately 'oversubtracted'. Subtraction of the five different candidate PSFs produces five distinct residual images which differ principally due to sampling variations (Fig. 4). In an attempt to minimize the production of artificial structure in the centre of the image, the median average of these five alternative residual images was used to produce the final host galaxy image for each quasar.

### 3.4 Images and aperture photometry

The final images of the quasars and their host galaxies are presented in Fig. 5; in general, due to the above-mentioned sampling problems, structure within a radius of $\simeq 2.5$ arcsec from the centre of the host galaxy images cannot be regarded as real. For comparison with the host galaxies, we have also obtained a deep $K$-band image of the $z = 0.184$ radio galaxy PKS 1215 − 033, and this is shown in Fig. 6.

The $K$ magnitudes of the quasars and their hosts were determined through an aperture of diameter 12 arcsec from the images presented in Fig. 5. This aperture was chosen for ease of comparison with the well-established $K$–$z$ relation for powerful radio galaxies (see Section 4). The results are given in Table 2. Obviously, since we have subtracted the entire nuclear PSF, the $K$ magnitudes of the host galaxies listed in Table 2 systematically underestimate their true brightness. The impact of alternative host galaxy models on the derived $K$ magnitudes will be discussed by Taylor et al. (in preparation), but the present approach does allow direct comparison of the $K$ magnitudes of RLQs and RQQs in an appealingly model-independent way.

Details on individual sources follow in the next section.

### 3.5 Notes on individual sources

In this section we provide a brief discussion of the $K$-band image of each quasar in the sample, with particular reference to any existing optical data. Sources are listed by IAU name,

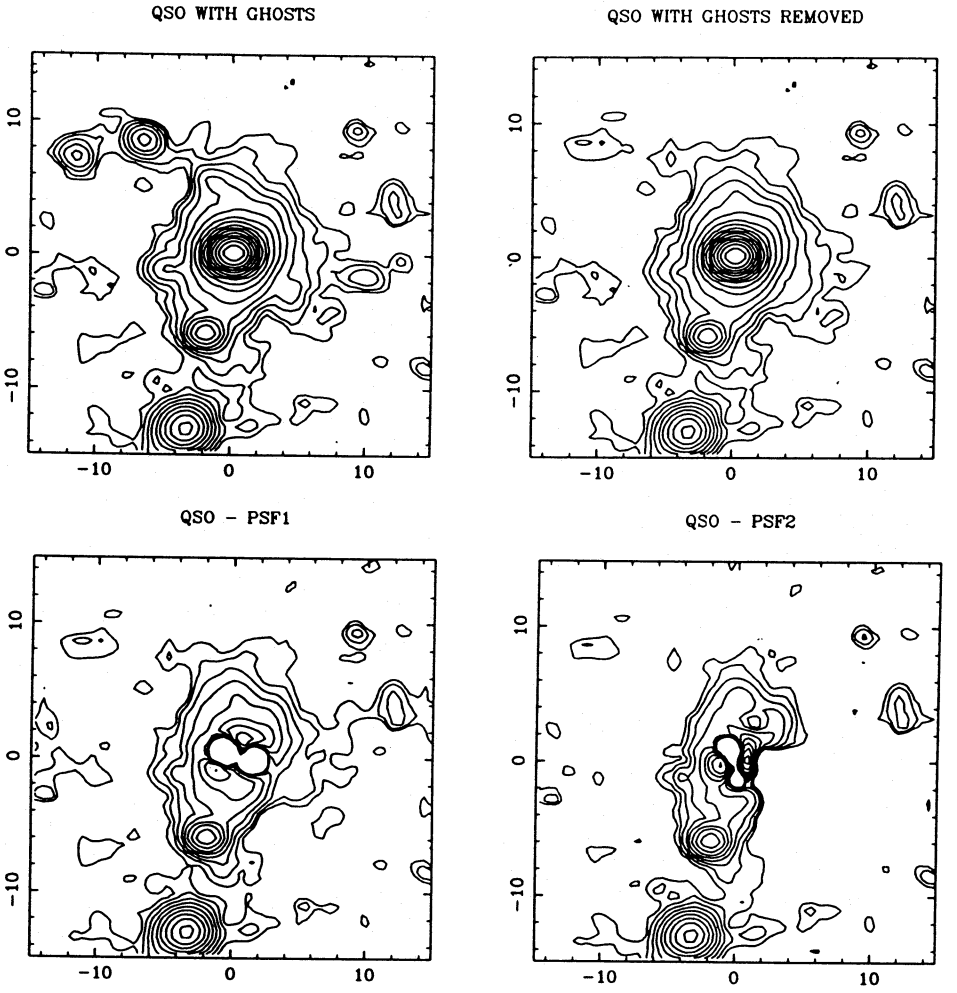


**Figure 4.** Illustration of the impact of ghost removal followed by subtraction of the five alternative PSFs from the quasar image (0052 + 251). The final image of the host galaxy is the median average. The figure illustrates the impact of sampling variations on the central region of the host-galaxy image. Contour intervals are $\Delta\mu_K = 0.5$ mag arcsec$^{-2}$, with the base contour corresponding to a surface brightness $\mu_K = 21.75$ mag arcsec$^{-2}$ above the sky. The images are 30 arcsec square, with north to the top and east to the left.

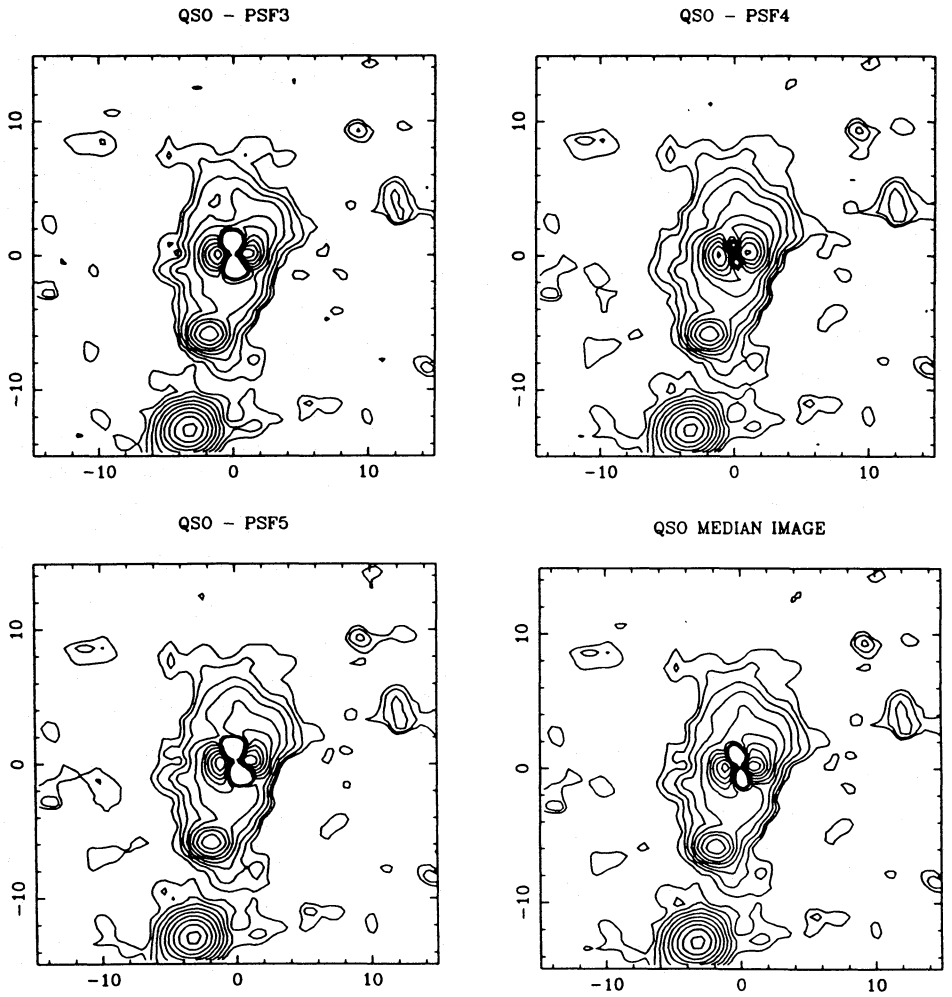


**Figure 4** – *continued*

with alternative names given in parentheses. Radio luminosities at 5 GHz have been calculated from the radio fluxes and spectral indices given in Table 1. Relative coordinates and $K$ magnitudes (5-arcsec aperture magnitudes) for all clearly detected 'companion' objects in the images are given in Table 3. The significance of these companions is discussed further in Section 4.4.

*0007+106 (III Zw 2)*

Radio-quiet [$z = 0.090$, $\log_{10}(L_{5\,\mathrm{GHz}}) = 23.89$]

The suspected spiral arm noted by Hutchings et al. (1984b) and Green, Williams & Morton (1978) is also seen here, but is less prominent. The extension to the NE of the nucleus is the remnant of a ghost image. We find three previously undetected compact 'companion' sources to the S, SE and W. That 0007+106 may lie within a group of galaxies is also suggested by the fact that Heckman et al. (1984) carried out imaging spectroscopy on a companion 40 kpc from the quasar (object 15 in Green & Yee 1984, beyond the field of view of our image) and found its redshift to agree with that of the quasar to within $10^3$ km s$^{-1}$.

*0046+112 (PHL 850)*

Radio-quiet ($z = 0.275$)

This image consists of only 45 min of integration instead of the 'standard' 54 min. The quasar is only marginally resolved, but there is evidence of extension to the NW. The image contains 'companion' objects to the SE and SW, but there is no evidence of association. Hutchings et al. (1989) indicate that 0046+112 appears to be in a group of galaxies.

*0052+251 (PG 0052+251)*

Radio-quiet [$z = 0.154$, $\log_{10}(L_{5\,\mathrm{GHz}}) = 21.78$]

Hutchings et al. (1989) describe this quasar as irregular with two nuclei. We confirm the double nucleus and bright, linked companion to the south. The image also contains compact companions to the NW and WNW of the main nucleus. Boroson et al. (1982) have shown that the nebulosity surrounding the nuclei is starlight. In the [O III] image by Stockton & MacKenty (1987), the brightest region of line emission lies 3.5 arcsec to the south of the quasar nucleus (i.e. between the quasar and the secondary nucleus to the south). Neuge-

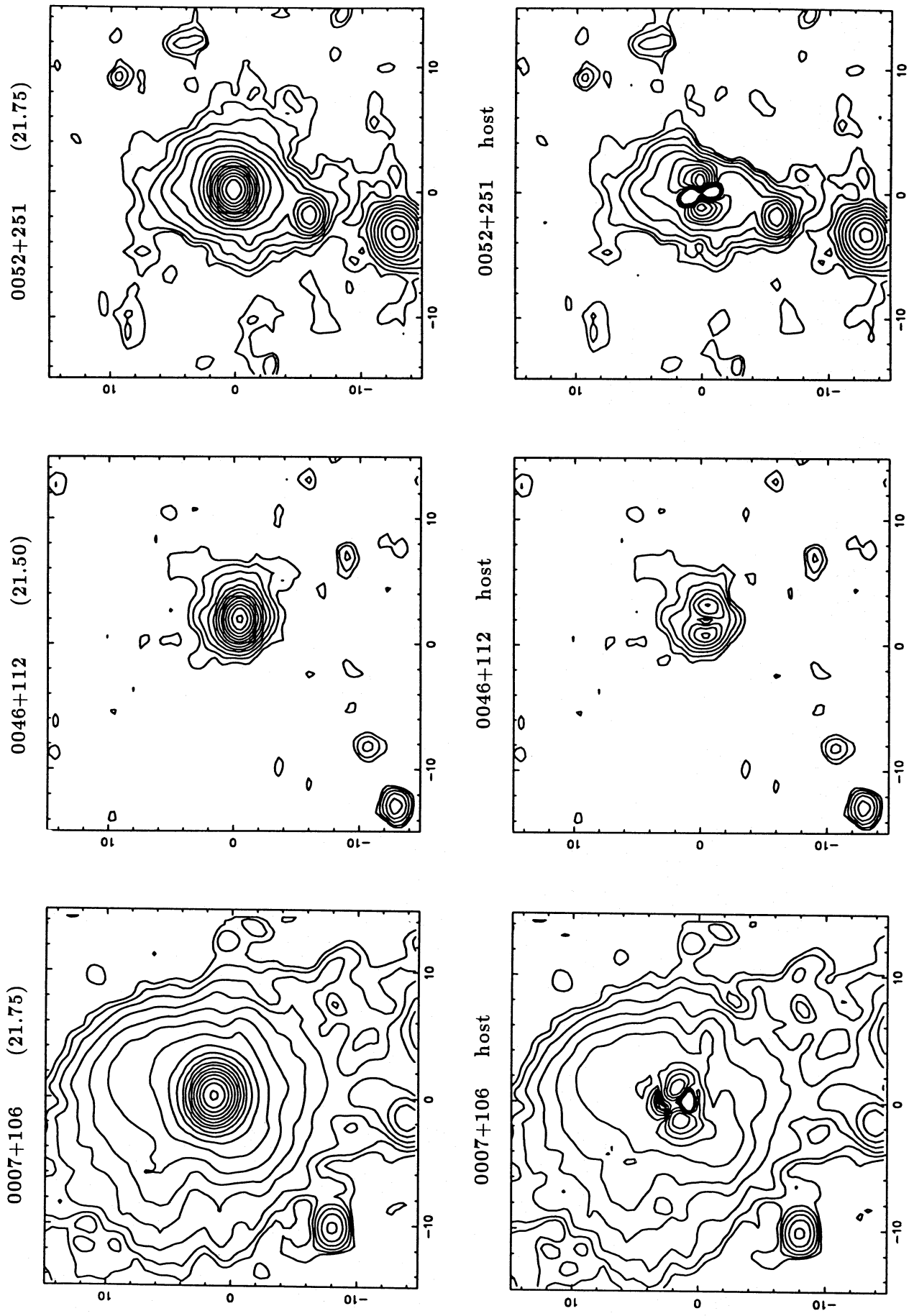


**Figure 5.** The final images of the quasars and their host galaxies, before and after subtraction of the central component. The surface brightness level of the base contour varies slightly from object to object, and is given in parentheses after the source name at the top of each plot. Contour intervals in all plots are $\Delta\mu_K = 0.5$ mag arcsec$^{-2}$. The images are 30 arcsec square, with north to the top and east to the left.

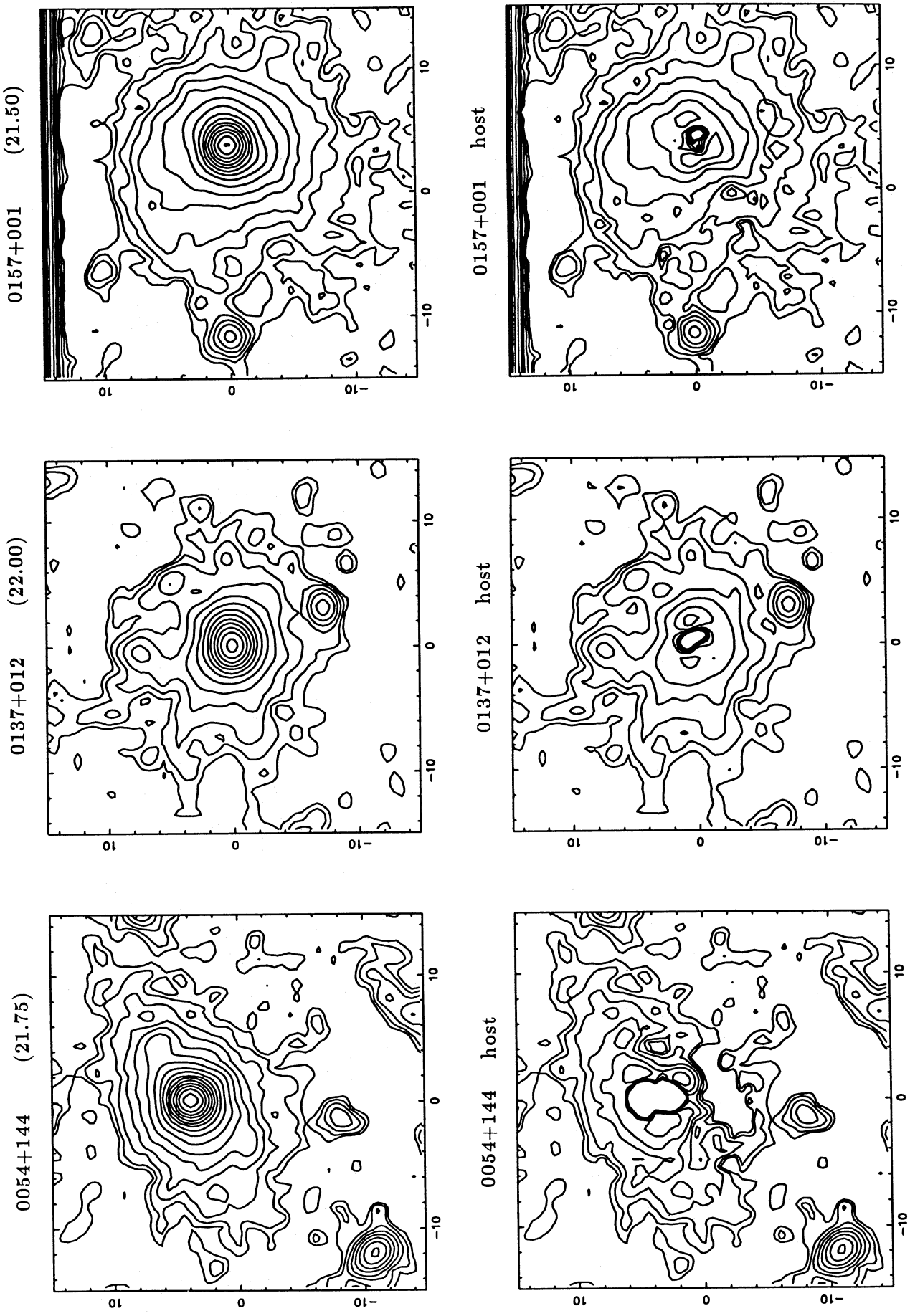


**Figure 5** - *continued*

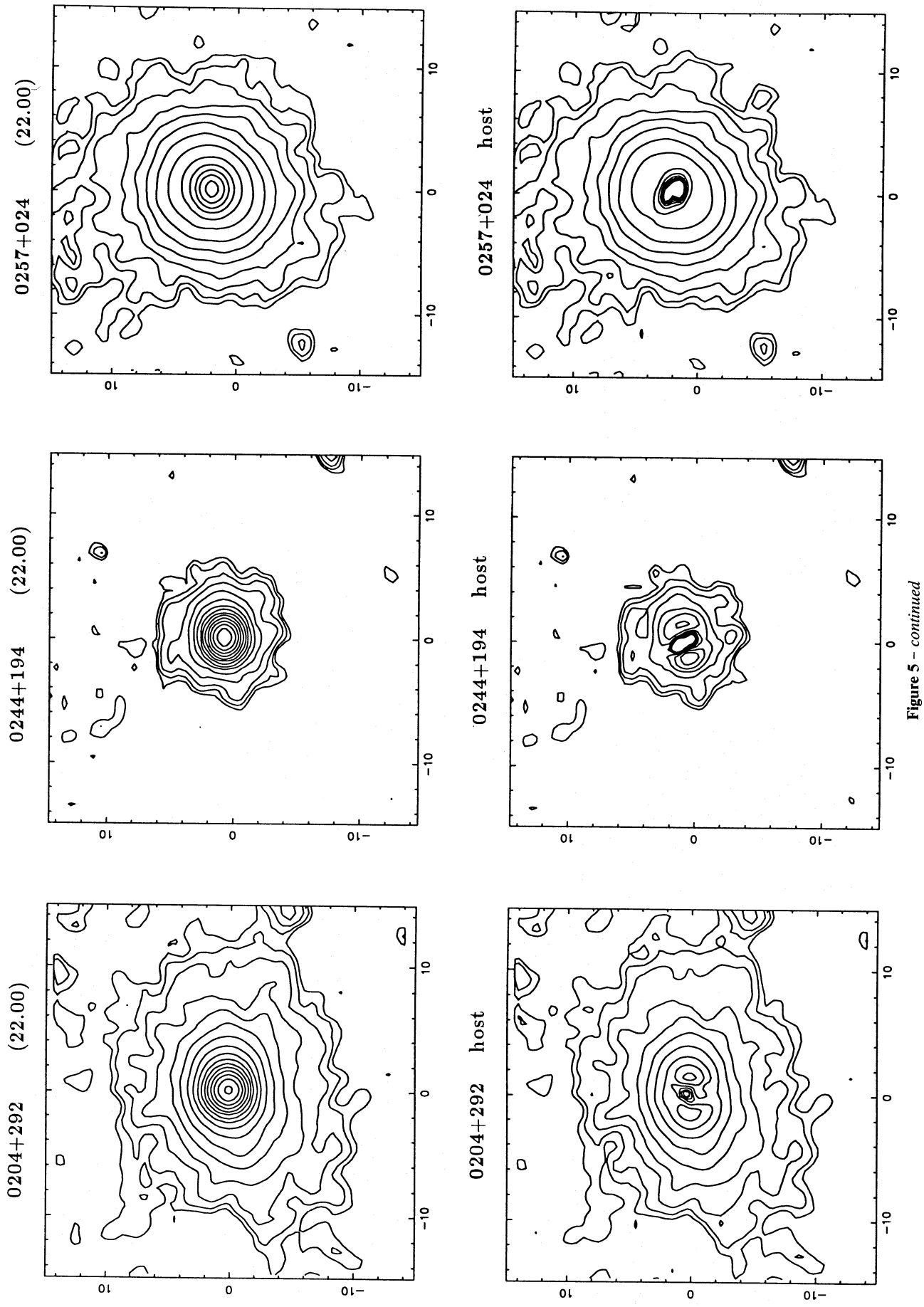


**Figure 5** – *continued*

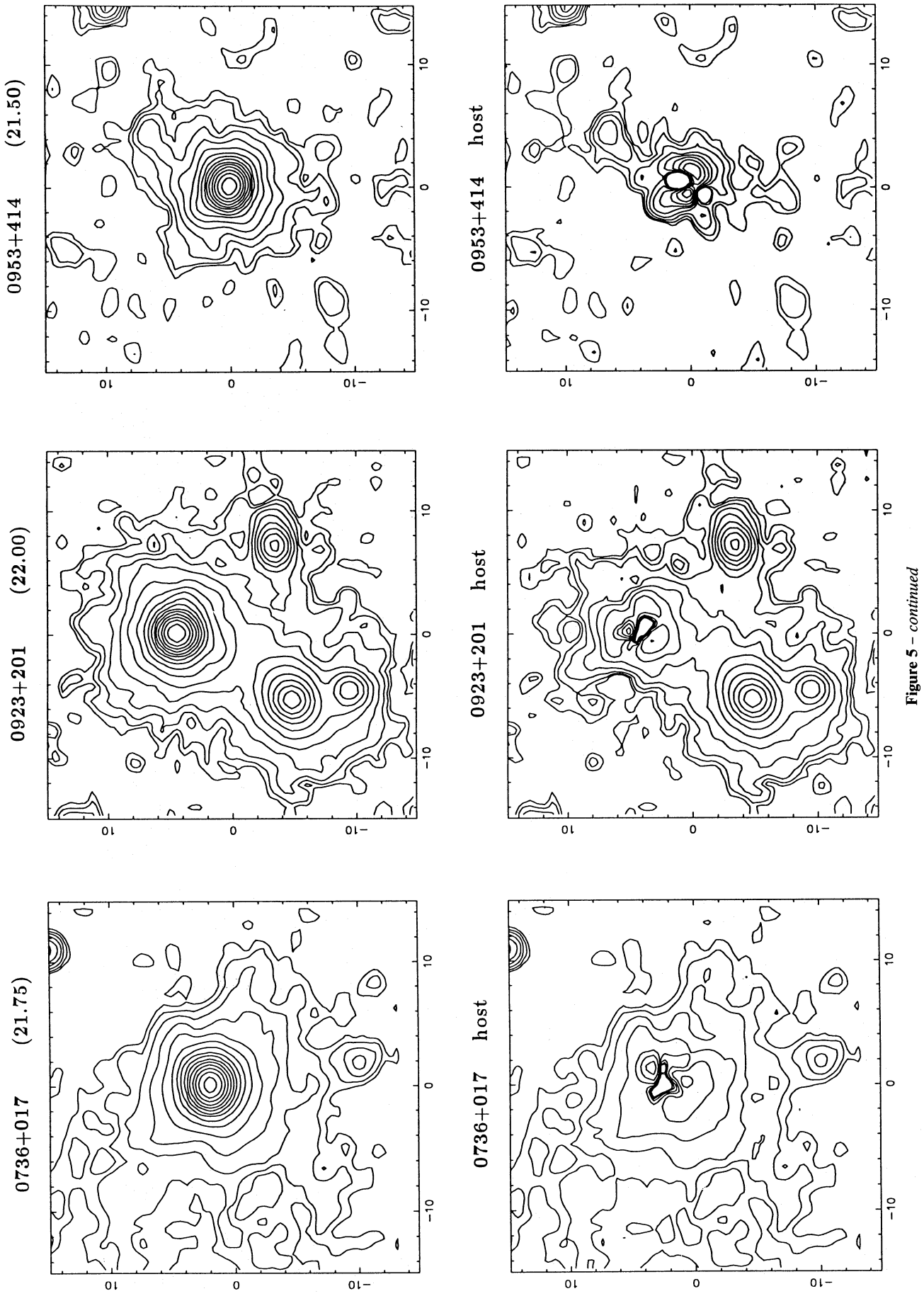


**Figure 5** – *continued*

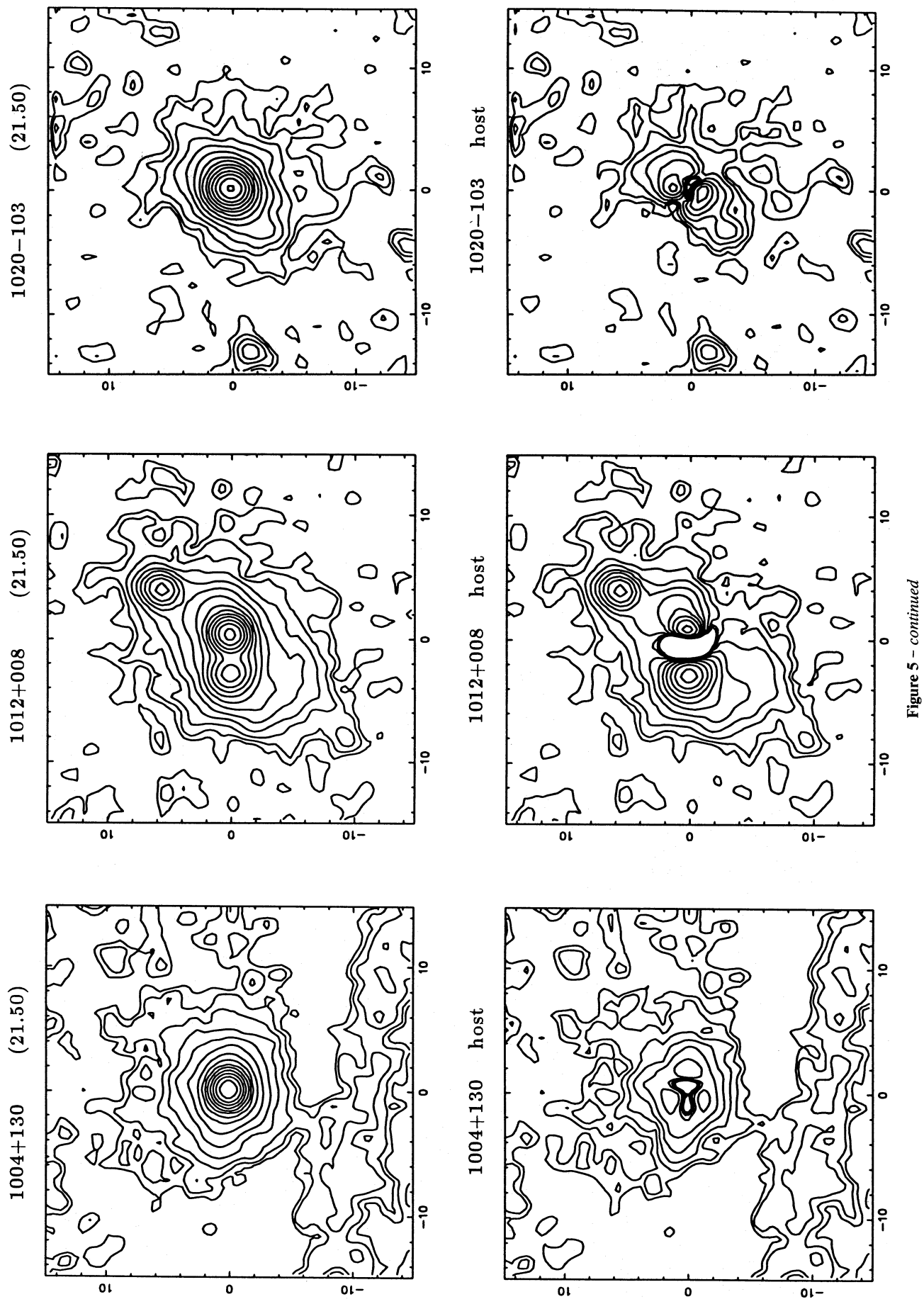


**Figure 5** – *continued*

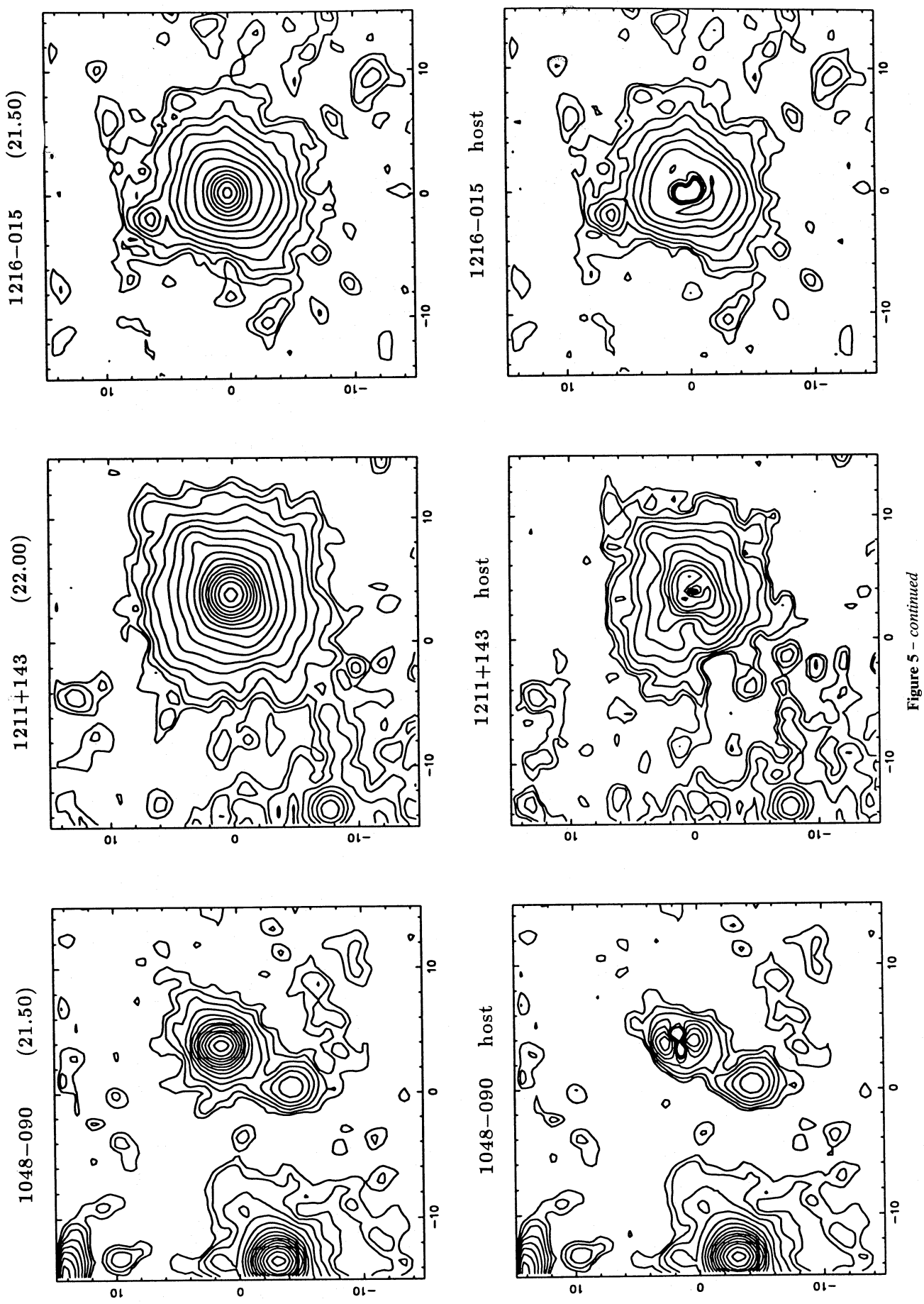


**Figure 5** – *continued*

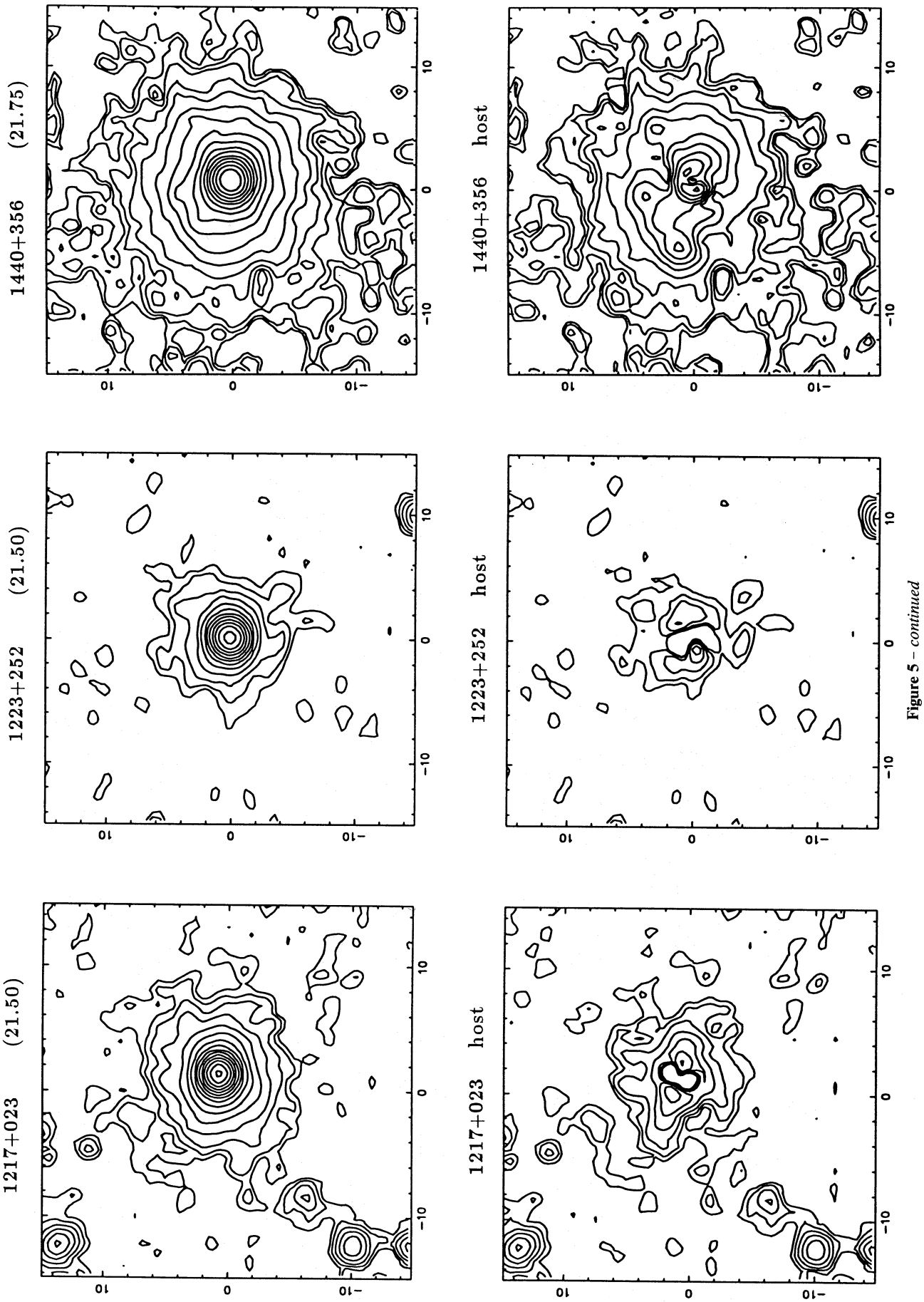


**Figure 5** – *continued*

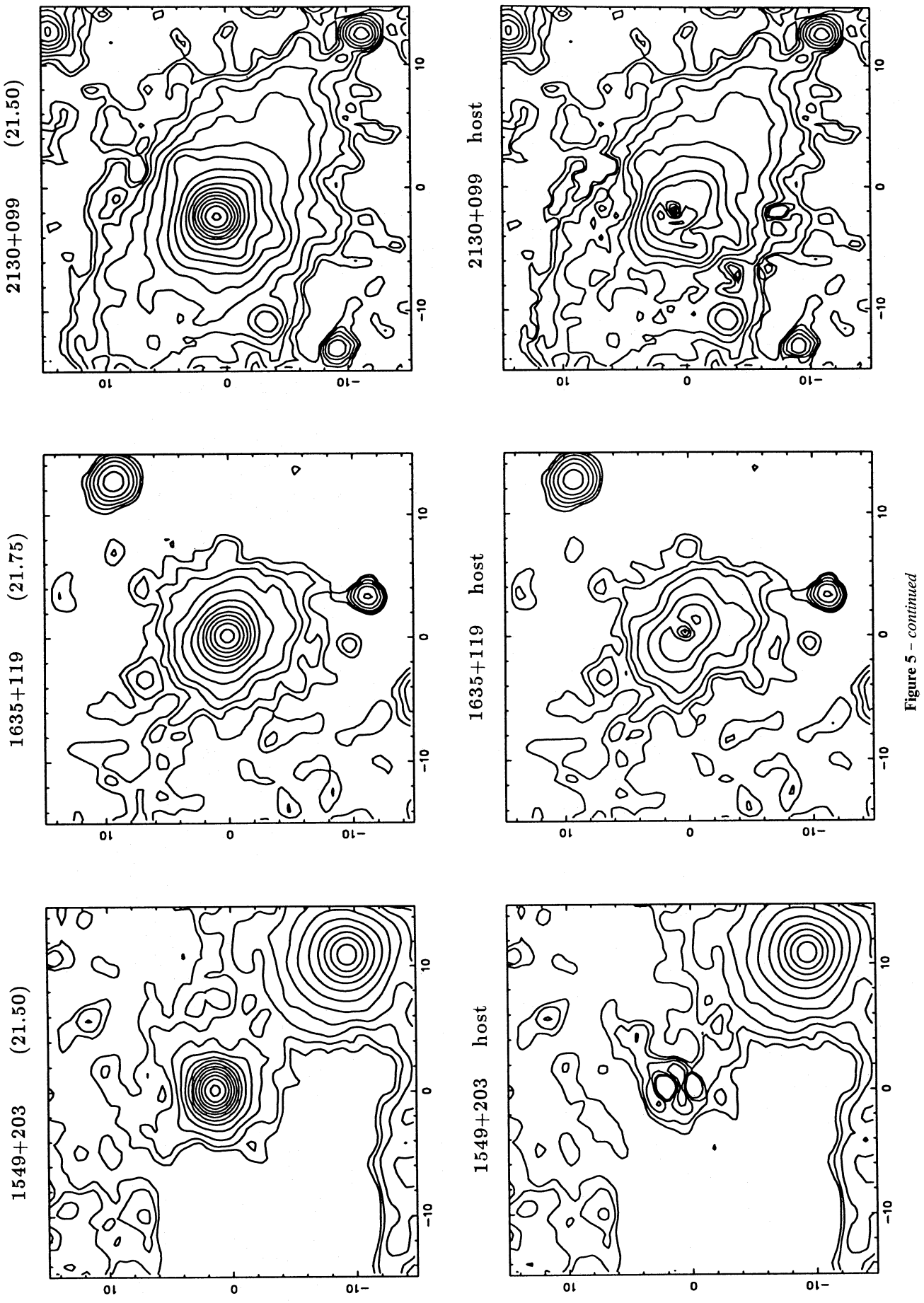


**Figure 5** – *continued*

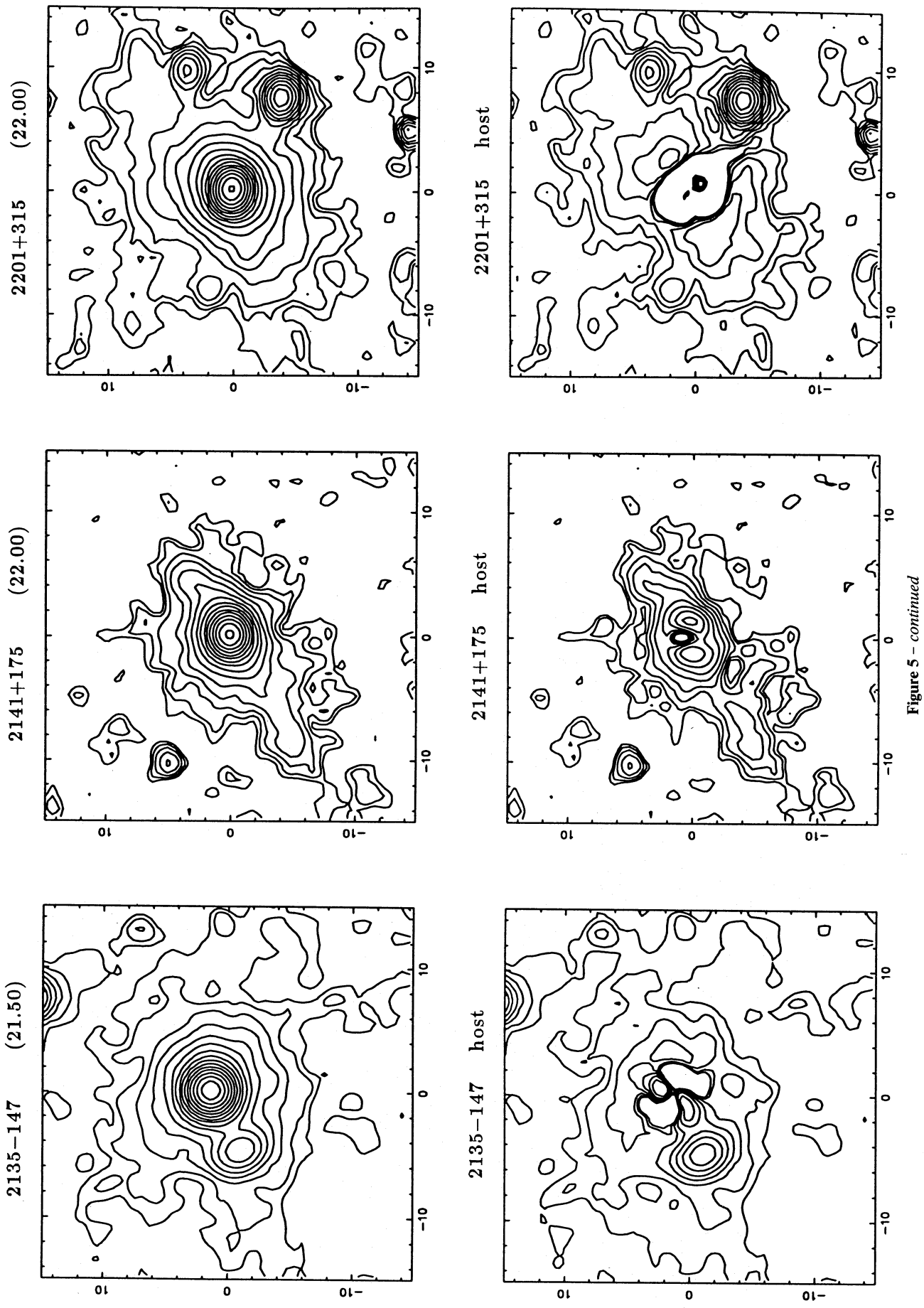


**Figure 5** – *continued*

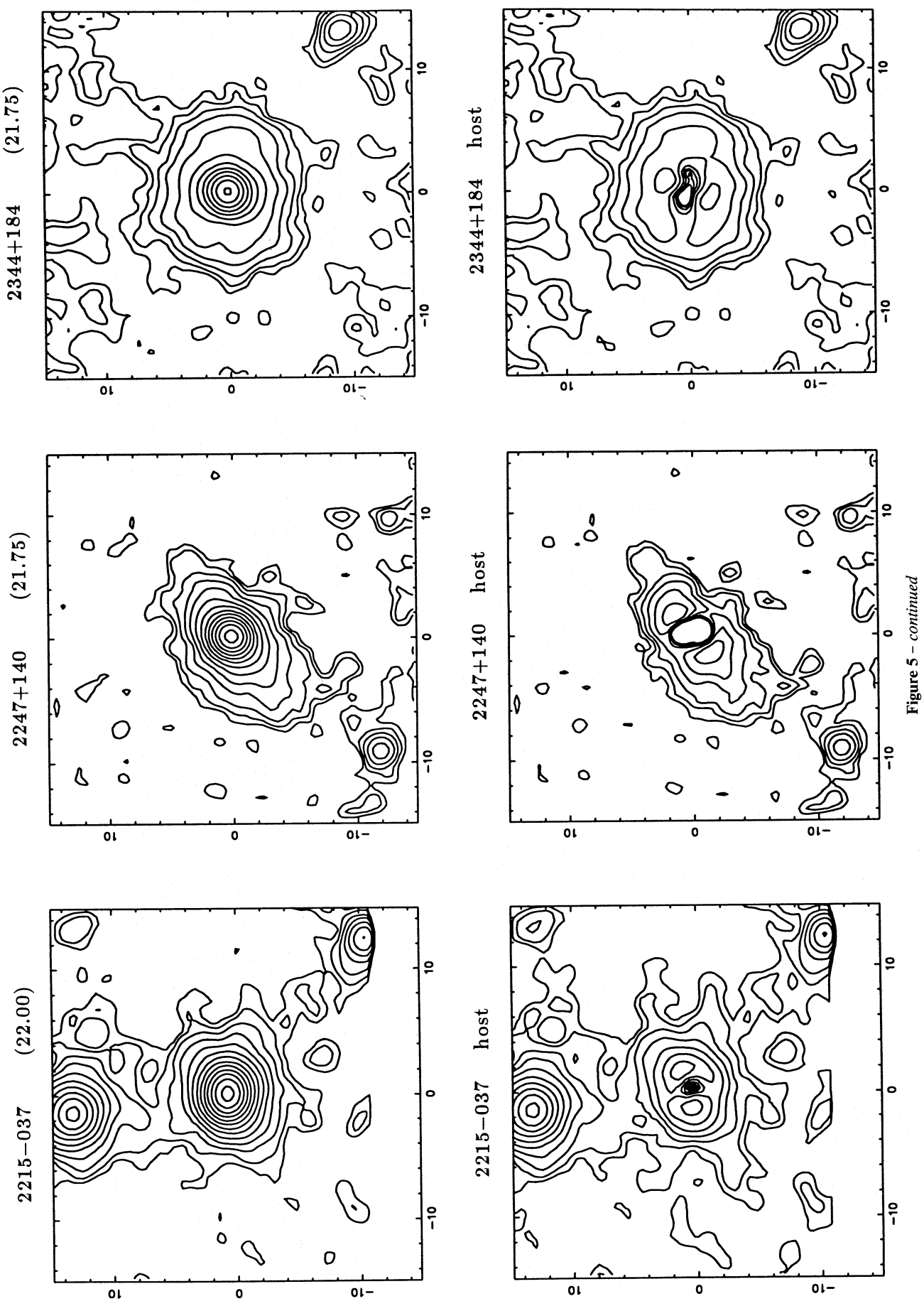


**Figure 5** – *continued*

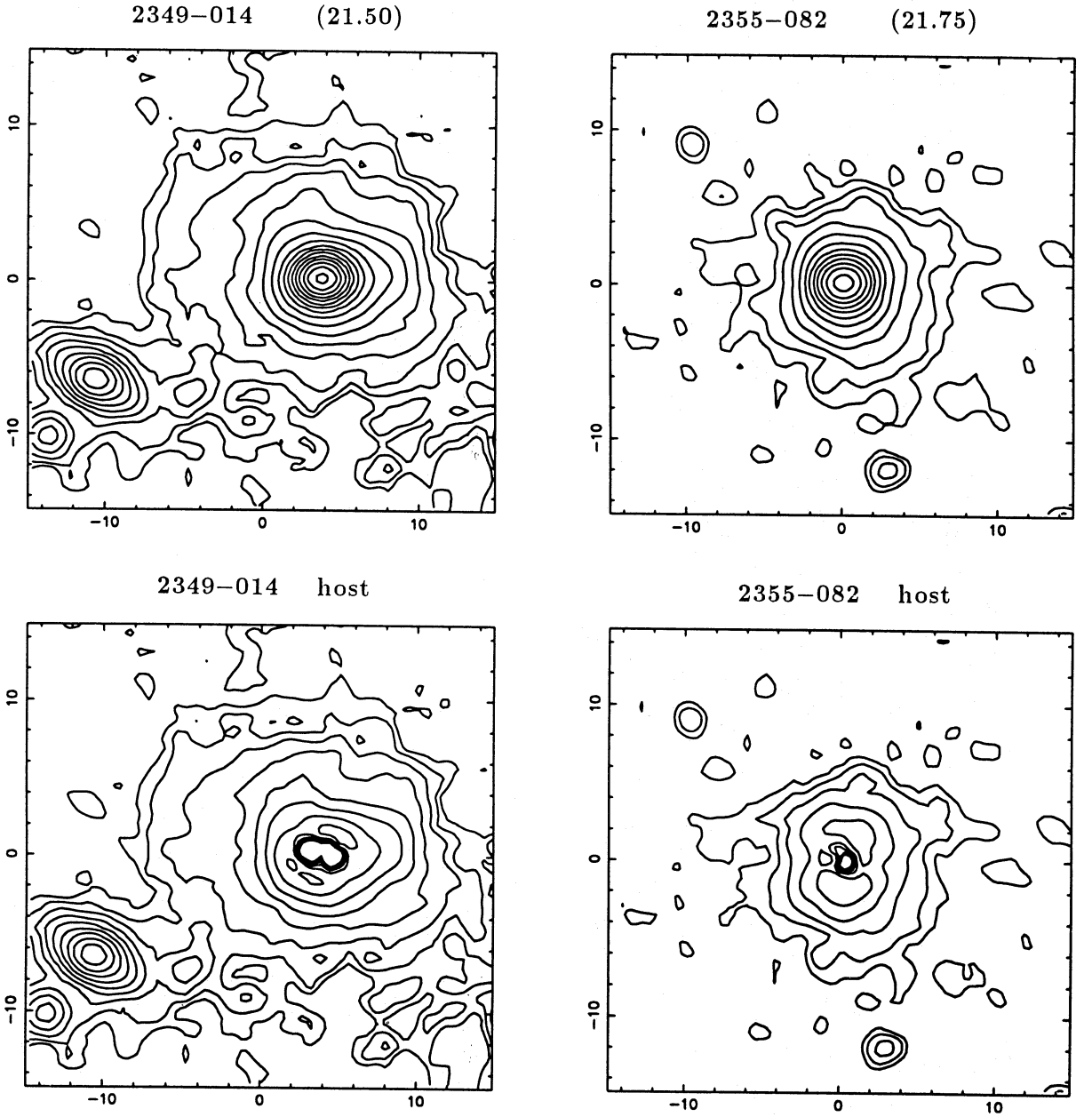


**Figure 5** – *continued*

bauer et al. (1987) give a spectral energy distribution for this object which is characterized by a power law from 3 to 0.9 μm, plus a '3000-Å bump'. The form of the continuum is very similar to that of 0157+001. Barvainis (1990) has argued that the spectrum can best be modelled by strong emission from galactic dust in the far-infrared and equal contributions of nuclear dust, starlight and 'big blue bump' (BBB) in the near-infrared.

*0054+144 (PHL 909)*

Radio-quiet ($z = 0.171$)

As in the optical image by Gehren et al. (1984), the galaxy appears extended towards the western companion (possibly due to tidal interaction), and three other obvious 'companions' exist to the S, SE and N (on the edge of the frame). Barvainis (1990) presented a spectral energy distribution for this object, which was well modelled by a nuclear dust component and a power law in the near-infrared to optical, but which turned upward towards longer wavelengths, resulting in a 100-μm excess (possibly due to cool dust in the host galaxy).

*0137+012 (PKS 0137+012, PHL 1093, 4C 01.04, OC 062, UM 355)*

Radio-quiet [$z = 0.258$, $\log_{10}(L_{5\,\mathrm{GHz}}) = 25.26$]

Our image confirms the presence of the two nearby 'companions' seen in the *V*-band image by Smith et al. (1986), both of which are embedded in the quasar's surrounding luminosity. In addition, we confirm the presence of an exten-

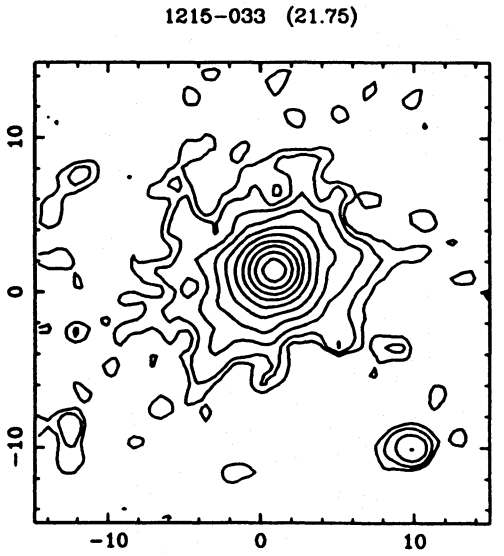


**Figure 6.** The *K*-band image of the 'control' radio galaxy PKS 1215−033 ($z=0.184$). As in Fig. 5, the surface brightness level of the base contour is given in parentheses above the figure, and contour intervals are $\Delta\mu_K=0.5$ mag arcsec$^{-2}$. The image is 30 arcsec square, with north to the top and east to the left.

sion to the ESE, but in our *K*-band image this points towards a red companion object (on the edge of the frame) which is undetected in the optical image. The extension to the NE may be an artefact, as this was a region frequently contaminated by ghost images; this extension does not appear in the *V*-band image of Smith et al. (1986). In the radio the quasar is an FRII source of diameter 42 arcsec, with a strong core (Gower & Hutchings 1984a).

*0157+001 (PG 0157+001, Mrk 1014)*

Radio-quiet [$z=0.162$, $\log_{10}(L_{5\,\mathrm{GHz}})=22.87$]

The host galaxy of this quasar is extremely large and luminous. Clearly seen is the eastern arm-like feature first noted by MacKenty & Stockton (1984). Smith et al. (1986) argue that this is probably due to tidal disruption, since they see no 'counter arm'. Despite the appearance of a second faint, arm-like feature to the NW in our *K*-band image, the tidal-tail interpretation is now strengthened by the compact objects that appear at the end of these arms in our *K*-band image (see also Section 4.5). Stockton & MacKenty (1987) detected [O III] 5007-Å emission from several regions completely unrelated to the structure seen in their optical continuum image; in a bright patch due east of the nucleus, and also in three discrete blobs to the west (coincident with the general region of emission leading to the NW companion in our frame). They also detected the arm-like feature in their [O III] image, but concluded that this was almost entirely due to continuum. Sanders, Scoville & Soifer (1988a) inferred the presence of abundant $H_2$ in 0157+001 from their detection of CO(1→0) emission at 2.6 mm, and an *r*-band CCD image was presented by Sanders et al. (1988b). This most recent optical image contains all the principal features visible at *K*, apart from the NE companion which seems to be unique to our *K*-band observation (although it is possibly just seen at $\mu_R\simeq 24$ in the combined *R*-band optical image stack of MacKenty & Stockton 1984). Off-nuclear spectroscopy of the eastern arm has been performed by Heckman et al. (1984). They found a redshift difference between this region and the quasar of $300\pm200$ km s$^{-1}$. More recently, Hutchings & Crampton (1990) obtained spectra of the regions that display [O III] 5007-Å emission in the narrow-band images taken by Stockton & MacKenty (1987). The spectra show absorption features matching emission-line redshifts to within the errors. The radio structure of this 'radio-quiet' quasar is similar to that found in several radio-loud quasars, with an unresolved core accompanied by a secondary component $\simeq 2$ arcsec west of the nucleus (Miller & Rawlings, private communication).

*0204+292 (3C59?)*

Radio-loud [$z=0.109$, $\log_{10}(L_{5\,\mathrm{GHz}})=24.55$]

The host galaxy of the quasar is well resolved, and there is a compact companion 15 arcsec to the WSW of the nucleus, apparently interacting with the host galaxy. Recent MERLIN observations by Meurs & Unger (1991) have shown that the radio source 3C59 appears to consist of three distinct sources, with the quasar 0204+292 being identified with the faintest of these ($S_{1415}=26$ mJy). A revised $S_{5\,\mathrm{GHz}}$ and radio spectral index have still to be determined, but it seems likely that this source will have to be re-classified as radio-quiet according to our 5-GHz luminosity criterion.

*0244+194 (1E 0244+1928)*

Radio-quiet ($z=0.176$)

Again, no deep optical CCD images of this quasar appear to exist in the literature. A single, unresolved object lies about 15 arcsec WSW of the nucleus.

*0257+024 (US 3498)*

Radio-quiet ($z=0.115$)

The isophotes of this host galaxy are almost circular, although there appears to be an extension to the luminosity on the north edge. A single companion lies about 15 arcsec to the SE. No deep optical CCD images are available for comparison.

*0736+017 (PKS 0736+01, OI 061)*

Radio-loud [$z=0.191$, $\log_{10}(L_{5\,\mathrm{GHz}})=25.35$]

The *K*-band image of this highly disturbed object contains the compact companions to the NW seen by both Hutchings, Johnson & Pyke (1988) and Smith et al. (1986) in their optical images. In addition, a previously undetected object lies to the south of the nucleus, embedded in the nebulosity surrounding the quasar. There is a large area of low surface brightness nebulosity extending to the NE. At radio wavelengths this quasar is a compact (0.013 arcsec), flat-spectrum source (Gower & Hutchings 1984b; Romney et al. 1984).

*0923+201 (PG 0923+201, Ton 1057)*

Radio-quiet [$z=0.190$, $\log_{10}(L_{5\,\mathrm{GHz}})=21.49$]

Hutchings et al. (1989) described this source as a possible interacting object lying in a group of galaxies. Heckman et al.

**Table 2.** *K*-band photometry of the quasars and their hosts. $K_{qso}$ is the *K* magnitude (within an aperture of diameter 12 arcsec) of the quasar (including its host) prior to subtraction of the scaled PSF. $K_{host}$ is the 12-arcsec diameter *K* magnitude after subtraction of the scaled PSF, prior to any correction being applied to compensate for the resulting inevitable oversubtraction of flux. The corrections applied in determining $M_{K(qso-host)}$, $M_{K(host)}$ and $L_{nuc}$:$L_{host}$ are described in Sections 4.1 and 4.2.

| Classification | Name | $K_{qso}$ | $K_{host}$ | $M_{K(qso-host)}$ | $M_{K(host)}$ | $L_{nuc} : L_{host}$ |
|---|---|---|---|---|---|---|
| **Radio Loud** | 0137+012 | 13.69±0.05 | 15.14±0.14 | −26.6 | −26.1 | 1.60 |
| | 0204+292 | 12.47±0.03 | 13.98±0.18 | −25.9 | −25.6 | 1.36 |
| | 0736+017 | 12.64±0.04 | 14.84±0.50 | −27.4 | −25.8 | 4.37 |
| | 1004+130 | 12.77±0.04 | 15.12±0.15 | −27.7 | −26.0 | 4.78 |
| | 1020−103 | 13.02±0.03 | 15.30±0.35 | −27.0 | −25.4 | 4.42 |
| | 1048−090 | 13.62±0.03 | 15.92±0.25 | −27.6 | −25.8 | 5.45 |
| | 1217+023 | 12.86±0.04 | 15.32±0.16 | −27.8 | −25.8 | 6.54 |
| | 1223+252 | 13.97±0.04 | 16.29±0.29 | −26.9 | −25.0 | 5.83 |
| | 2135−147 | 12.17±0.03 | 14.75±0.30 | −28.0 | −26.0 | 6.36 |
| | 2141+175 | 13.06±0.03 | 14.96±0.10 | −27.1 | −25.9 | 3.06 |
| | 2201+315 | 12.14±0.03 | 15.00±0.25 | −29.1 | −26.5 | 11.36 |
| | 2247+140 | 13.52±0.03 | 15.23±0.20 | −26.8 | −25.8 | 2.41 |
| | 2349−014 | 12.12±0.03 | 13.98±0.23 | −27.6 | −26.5 | 2.68 |
| | 2355−082 | 13.87±0.03 | 15.31±0.14 | −25.9 | −25.5 | 1.43 |
| **Radio Quiet** | 0007+106 | 11.46±0.03 | 13.43±0.28 | −26.8 | −25.7 | 2.68 |
| | 0046+112 | 13.70±0.03 | 15.85±0.15 | −27.6 | −25.7 | 6.10 |
| | 0052+251 | 12.20±0.03 | 15.14±0.35 | −27.6 | −25.1 | 9.49 |
| | 0054+144 | 12.27±0.03 | 14.40±0.20 | −27.5 | −26.1 | 3.85 |
| | 0157+001 | 12.15±0.03 | 13.63±0.15 | −27.1 | −26.7 | 1.42 |
| | 0244+194 | 13.45±0.03 | 15.62±0.18 | −26.4 | −24.9 | 4.20 |
| | 0257+024 | 13.12±0.03 | 13.81±0.05 | −23.1 | −25.9 | 0.08 |
| | 0923+201 | 12.33±0.03 | 14.95±0.20 | −27.7 | −25.7 | 6.03 |
| | 0953+414 | 12.44±0.03 | 15.28±0.15 | −28.1 | −25.8 | 8.46 |
| | 1012+008 | 12.62±0.03 | 13.94±0.15 | −26.3 | −26.7 | 0.73 |
| | 1211+143 | 11.74±0.03 | 13.56±0.15 | −26.1 | −25.5 | 1.66 |
| | 1216−015 | 12.78±0.03 | 14.08±0.05 | −24.8 | −25.4 | 0.59 |
| | 1440+356 | 11.69±0.03 | 13.32±0.25 | −26.1 | −25.6 | 1.53 |
| | 1549+203 | 13.56±0.09 | 15.99±0.28 | −27.2 | −25.2 | 6.66 |
| | 1635+119 | 13.79±0.04 | 15.16±0.41 | −25.2 | −25.0 | 1.18 |
| | 2130+099 | 11.43±0.03 | 13.03±0.15 | −25.8 | −25.4 | 1.46 |
| | 2215−037 | 13.57±0.03 | 14.98±0.14 | −26.5 | −26.1 | 1.40 |

(1984) carried out spectroscopy of the two interacting companions to the SE and SW and found strong absorption lines characteristic of an old stellar population. The redshifts of the absorption lines match the quasar redshift to within $10^3$ km $s^{-1}$.

*0953+415 (K438−7, PG 0923+415)*

Radio-quiet [$z = 0.239$, $\log_{10}(L_{5\,GHz}) = 22.57$]

There are two clearly detected 'companions' to the NW, one close to the nucleus, the other ~18 arcsec distant on the edge of the frame. Several other fainter 'companions' may also be present. Hutchings et al. (1989) claim that this quasar is possibly interacting, is part of a group of galaxies, has spiral structure and has a possible tidal tail. Boroson et al. (1985) have taken both nuclear and off-nuclear spectra of this quasar. They found the host galaxy spectrum to be dominated by a red continuum with S II and H$\alpha$ emission, and a possible Mg Ib absorption feature.

*1004+130 (PKS 1004+13, PG 1004+130, 4C 13.41, OL 107.7)*

Radio-loud [$z = 0.240$, $\log_{10}(L_{5\,GHz}) = 24.94$]

The bright arc across the lower portion of this image is scattered light from a nearby bright star. The host galaxy

**Table 3.** Relative positions and *K*-band photometry of 'companions'. Companion magnitudes have been determined through an aperture of diameter 5 arcsec. For each quasar, companions have been ranked in terms of projected distance from the central source.

| Source Name | Companion No. | ΔRA (″) | ΔDec (″) | *K* |
|---|---|---|---|---|
| **0007+106** | Comp. 1 | 10.5 | −9.3 | 17.75 ± 0.25 |
| | Comp. 2 | 1.2 | −14.9 | 17.05 ± 0.15 |
| | Comp. 3 | 18.0 | 6.2 | 19.05 ± 0.20 |
| **0046+112** | Comp. 1 | −5.0 | −8.7 | 19.00 ± 0.25 |
| | Comp. 2 | 10.5 | −10.5 | 18.90 ± 0.15 |
| | Comp. 3 | −3.7 | −17.4 | 17.40 ± 0.20 |
| | Comp. 4 | 14.9 | −12.4 | 18.10 ± 0.10 |
| **0052+251** | Comp. 1 | 1.9 | −6.2 | 16.05 ± 0.03 |
| | Comp. 2 | −12.4 | 3.7 | 18.65 ± 0.30 |
| | Comp. 3 | −9.3 | 9.3 | 19.75 ± 0.50 |
| | Comp. 4 | 3.7 | −13.0 | 15.77 ± 0.02 |
| | Comp. 5 | 1.9 | 17.4 | 16.55 ± 0.03 |
| | Comp. 6 | 19.8 | 5.6 | 15.92 ± 0.02 |
| **0054+144** | Comp. 1 | 1.2 | −11.8 | 18.15 ± 0.20 |
| | Comp. 2 | 1.2 | 11.8 | 18.72 ± 0.08 |
| | Comp. 3 | −15.5 | 3.7 | 17.40 ± 0.06 |
| | Comp. 4 | 12.4 | −14.9 | 16.48 ± 0.07 |
| **0137+012** | Comp. 1 | −5.0 | 4.3 | 18.35 ± 0.20 |
| | Comp. 2 | 0.6 | 7.4 | 18.05 ± 0.25 |
| | Comp. 3 | −3.1 | −7.4 | 17.73 ± 0.06 |
| | Comp. 4 | 15.5 | −5.6 | 18.60 ± 0.07 |
| | Comp. 5 | −13.0 | 14.9 | 19.70 ± 0.15 |
| **0157+001** | Comp. 1 | −8.1 | −3.7 | 18.10 ± 0.40 |
| | Comp. 2 | 9.9 | 9.9 | 18.50 ± 0.20 |
| | Comp. 3 | −9.3 | 10.5 | 18.05 ± 0.15 |
| | Comp. 4 | 15.5 | 0.00 | 17.20 ± 0.25 |
| | Comp. 5 | 6.2 | −19.2 | 17.75 ± 0.15 |
| | Comp. 6 | 11.8 | −19.2 | 16.92 ± 0.02 |
| **0204+292** | Comp. 1 | −14.9 | −4.3 | 18.20 ± 0.25 |
| | Comp. 2 | 16.1 | 6.8 | 19.00 ± 0.12 |
| **0244+193** | Comp. 1 | −14.9 | −8.7 | 18.30 ± 0.20 |
| **0257+024** | Comp. 1 | 12.4 | −7.4 | 19.40 ± 0.50 |
| **0736+017** | Comp. 1 | −1.9 | −12.4 | 17.95 ± 0.25 |
| | Comp. 2 | −10.5 | 13.0 | 17.40 ± 0.10 |
| **0923+201** | Comp. 1 | −6.8 | −8.1 | 16.20 ± 0.08 |
| | Comp. 2 | 5.6 | −9.3 | 14.83 ± 0.05 |
| | Comp. 3 | 5.0 | −13.6 | 16.30 ± 0.15 |
| | Comp. 4 | 16.1 | 8.7 | 17.75 ± 0.07 |
| | Comp. 5 | −19.8 | 1.9 | 20.05 ± 0.20 |

**Table 3** – *continued*

| Source Name | Companion No. | ΔRA (″) | ΔDec (″) | *K* |
|---|---|---|---|---|
| **0953+415** | Comp. 1 | −4.3 | 6.2 | 17.70 ± 0.25 |
| | Comp. 2 | 9.3 | −8.1 | 18.40 ± 0.30 |
| | Comp. 3 | −14.9 | 9.9 | 17.05 ± 0.05 |
| **1012+008** | Comp. 1 | −3.7 | 5.6 | 15.68 ± 0.03 |
| | Comp. 2 | 8.1 | −9.3 | 18.30 ± 0.25 |
| | Comp. 3 | −18.6 | −16.1 | 18.45 ± 0.45 |
| **1020−103** | Comp. 1 | 13.0 | −1.9 | 18.20 ± 0.25 |
| | Comp. 2 | 4.3 | −14.3 | 19.50 ± 0.50 |
| **1048−090** | Comp. 1 | 3.1 | −5.6 | 16.65 ± 0.02 |
| | Comp. 2 | −13.6 | 0.6 | 18.55 ± 0.25 |
| | Comp. 3 | 17.4 | −4.3 | 12.90 ± 0.02 |
| | Comp. 4 | 17.4 | 8.1 | 18.35 ± 0.25 |
| | Comp. 5 | 18.0 | 13.0 | 15.47 ± 0.02 |
| | Comp. 6 | 9.3 | −20.5 | 17.85 ± 0.10 |
| **1211+143** | Comp. 1 | 8.1 | 13.0 | 19.30 ± 0.50 |
| | Comp. 2 | −11.2 | −12.4 | 18.90 ± 0.45 |
| | Comp. 3 | 18.0 | −8.1 | 16.95 ± 0.11 |
| **1215−033 (RG)** | Comp. 1 | −9.3 | −11.8 | 18.40 ± 0.15 |
| | Comp. 2 | −2.5 | −19.2 | 18.50 ± 0.15 |
| **1216−015** | Comp. 1 | 1.9 | 6.2 | 17.55 ± 0.20 |
| | Comp. 2 | 10.5 | −3.1 | 18.35 ± 0.15 |
| | Comp. 3 | −9.3 | −11.8 | 18.27 ± 0.20 |
| | Comp. 4 | −11.2 | −16.7 | 19.90 ± 0.25 |
| **1217−023** | Comp. 1 | 9.9 | −6.8 | 18.22 ± 0.04 |
| | Comp. 2 | 6.2 | 10.5 | 19.20 ± 0.35 |
| | Comp. 3 | 13.6 | −11.1 | 17.38 ± 0.04 |
| | Comp. 4 | 13.6 | 13.0 | 17.30 ± 0.06 |
| **1223+252** | Comp. 1 | 16.1 | 6.2 | 18.70 ± 0.15 |
| | Comp. 2 | −9.9 | −14.9 | 17.95 ± 0.05 |
| **1440+356** | Comp. 1 | 16.1 | 2.5 | 17.70 ± 0.15 |
| **1549+203** | Comp. 1 | 9.9 | −5.0 | 18.15 ± 0.40 |
| | Comp. 2 | −5.6 | 9.9 | 18.60 ± 0.25 |
| | Comp. 3 | 9.9 | 6.2 | 17.55 ± 0.30 |
| | Comp. 4 | −11.2 | −10.5 | 14.07 ± 0.01 |
| **1635+119** | Comp. 1 | −3.7 | −11.8 | 17.90 ± 0.35 |
| | Comp. 2 | −12.4 | 9.3 | 17.01 ± 0.02 |
| | Comp. 3 | 4.3 | −15.5 | 17.95 ± 0.05 |
| **2130+099** | Comp. 1 | 8.7 | −4.3 | 17.00 ± 0.20 |
| | Comp. 2 | 11.2 | −9.9 | 17.73 ± 0.15 |
| | Comp. 3 | −15.5 | −11.8 | 16.95 ± 0.07 |
| | Comp. 4 | −15.5 | 13.6 | 16.33 ± 0.02 |

**Table 3** – *continued*

| Source Name | Companion No. | ΔRA (″) | ΔDec (″) | $K$ |
|---|---|---|---|---|
| **2135−147** | Comp. 1 | 5.0 | −2.5 | 16.00 ± 0.15 |
| | Comp. 2 | −13.0 | 5.6 | 19.80 ± 0.50 |
| | Comp. 3 | −7.4 | 14.3 | 17.83 ± 0.06 |
| | Comp. 4 | 16.7 | −9.3 | 17.00 ± 0.18 |
| **2141+175** | Comp. 1 | 7.4 | 8.7 | 19.30 ± 0.50 |
| | Comp. 2 | 10.5 | 5.0 | 18.60 ± 0.18 |
| | Comp. 3 | 18.0 | −1.9 | 18.60 ± 0.30 |
| **2201+315** | Comp. 1 | 8.1 | 1.9 | 18.43 ± 0.25 |
| | Comp. 2 | −7.4 | −3.7 | 15.13 ± 0.03 |
| | Comp. 3 | −9.3 | 3.7 | 17.45 ± 0.18 |
| | Comp. 4 | −5.0 | −14.9 | 18.08 ± 0.10 |
| | Comp. 5 | 17.4 | −4.3 | 19.00 ± 0.10 |
| **2215−037** | Comp. 1 | 1.9 | 13.0 | 15.16 ± 0.02 |
| | Comp. 2 | −12.4 | −11.2 | 17.30 ± 0.15 |
| | Comp. 3 | −13.0 | 12.4 | 18.53 ± 0.12 |
| **2247−140** | Comp. 1 | 9.3 | −12.4 | 17.71 ± 0.06 |
| | Comp. 2 | −9.9 | −13.0 | 18.70 ± 0.50 |
| **2344+184** | Comp. 1 | −13.0 | −9.3 | 17.35 ± 0.04 |
| | Comp. 2 | 16.1 | −7.4 | 19.45 ± 0.50 |
| | Comp. 3 | −11.2 | −18.0 | 17.90 ± 0.10 |
| | Comp. 4 | −17.4 | −18.0 | 16.84 ± 0.04 |
| **2349−014** | Comp. 1 | 5.0 | −9.3 | 19.10 ± 0.50 |
| | Comp. 2 | 8.7 | −7.4 | 17.90 ± 0.25 |
| | Comp. 3 | 14.9 | −6.8 | 15.24 ± 0.01 |
| | Comp. 4 | 17.4 | −10.5 | 17.25 ± 0.20 |
| **2355−082** | Comp. 1 | −2.5 | −12.4 | 19.05 ± 0.12 |
| | Comp. 2 | −14.3 | −16.7 | 17.82 ± 0.02 |
| | Comp. 3 | 19.2 | −14.9 | 18.50 ± 0.05 |

shows little structure although, as in the CCD image of Hutchings et al. (1988), the outer isophotes appear filamentary. However, we do not see the faint outer shell to the NW of the nucleus. Stockton & MacKenty (1987) presented narrow-band [O III] images of this quasar, but did not find any significant extended luminosity. Our $K$-band image contains no clearly detected companions (and so this source does not feature in Table 3), but this may well be due to the serious contamination of the image by scattered light. In the radio this quasar is an FRII source of diameter 9 arcmin, with a weak core (Miley & Hartsuijker 1978).

*1012+008 (PG 1012+00)*

Radio-quiet [$z = 0.185$, $\log_{10}(L_{5\,\mathrm{GHz}}) = 22.07$]

This complex source has two secondary nuclei plus several possible fainter compact companions. Hutchings et al. (1989) noted the evidence for interaction. They listed three secondary nuclei, but only give projected separations for the two nearest to the quasar. Heckman et al. (1984) give spectra for two of the companion objects, which contain the expected absorption lines at the quasar redshift.

*1020−103 (PKS 1020−103, UT 1020−103, OL−133, MSH 10−17)*

Radio-loud [$z = 0.197$, $\log_{10}(L_{5\,\mathrm{GHz}}) = 24.73$]

Three possible companions are visible in this image, to the E, S and SSE of the quasar nucleus. The quasar lies in a somewhat asymmetric host galaxy, which appears to be swept towards the SW. Comparison with the optical image shown in Hutchings et al. (1988) confirms the two companions to the S and SSE, whilst an extension is visible near the site of the third. An earlier optical image presented by Hutchings et al. (1984) does not show any of the companions nor the extended object. In all images the nucleus is off-centre. The radio source is core-dominated, with a single lobe $\simeq 2$ arcsec from the nucleus (Gower & Hutchings 1984b).

*1048−090 (3C 246, NRAO 359, OL−082, MSH 10−019, PG 1048−090, PKS 1048−09)*

Radio-loud [$z = 0.345$, $\log_{10}(L_{5\,\mathrm{GHz}}) = 25.50$]

The quasar nucleus is the brighter of the two central objects. The extended object to the south is clearly linked to the quasar, and there is an apparent tidal tail extending west of the group. This latter feature is not visible in the optical CCD image of Hutchings et al. (1988). In the radio the quasar is an FRII source of diameter 10 arcmin, with a clearly detected core (Miley & Hartsuijker 1978).

*1211+143 (PG 1211+143)*

Radio-quiet [$z = 0.085$, $\log_{10}(L_{5\,\mathrm{GHz}}) = 23.59$]

This appears to be the first deep electronic image to be taken of this object. It shows a companion galaxy apparently linked to the quasar host by nebulosity, and an unresolved object to the NNE.

*1216−015 (Mrk 1320)*

Radio-quiet ($z = 0.103$)

There is very little information in the literature on this quasar. The host galaxy appears fairly round, although the outer isophotes display filamentary structure. There is a close 'companion' to the NNE of the nucleus, and several possible fainter companions.

*1217+023 (PKS 1217+02, ON 029, UM 492)*

Radio-loud [$z = 0.240$, $\log_{10}(L_{5\,\mathrm{GHz}}) = 24.92$]

Six companions are visible on the $K$-band image, three to the NE and a line of three extending to the SE ($K$ magnitudes for

only four of these are given in Table 3, because two lie on the edge of the image). All six are also visible in the *R*-band image of Hutchings et al. (1988). The radio source is core-dominated, with a single lobe ≃ 20 arcsec from the nucleus (Dunlop et al. 1989).

*1223+252 (TON 616, 4C 2540, VR 25.12.02, ON 239, B2 1223+25)*

Radio-loud [$z = 0.268$, $\log_{10}(L_{5\,\mathrm{GHz}}) = 24.52$]

There is a slight extension to the SW towards the companion 18 arcsec distant. Neither of the two nearby (≃ 8 arcsec distant) 'companions' seen in the optical CCD images of Hutchings et al. (1988) and Hutchings & McClure (1990) are visible in our *K*-band image. In the radio the quasar is an FRII source of diameter 115 arcsec, with a clearly detected core (Miley & Hartsuijker 1978).

*1440+356 (Mrk 478, PG 1440+356, KW 42)*

Radio-quiet [$z = 0.079$, $\log_{10}(L_{5\,\mathrm{GHz}}) = 21.55$]

The host of this low-redshift quasar covers most of the image. The galaxy has a generally round appearance, with a possible bright spot detected in the star-subtracted image 4 arcsec east of the nucleus.

*1549+203 (LB 906, 1E 15498+203)*

Radio-quiet ($z = 0.250$)

This is the first deep electronic image of this quasar. There appears to be an interaction between the quasar host and the galaxy to the SW, but the situation is confused by the presence of a nearby, foreground galaxy cluster ($z = 0.135$; Stocke et al. 1983).

*1635+119 (MC 2)*

Radio-quiet [$z = 0.146$, $\log_{10}(L_{5\,\mathrm{GHz}}) = 23.77$]

A thin extension is seen NE of this source. Two of the four 'companions' seen by Malkan (1984) are visible on the image (the other two lie beyond the IRCAM field of view). These two companions are also seen in the optical image of Hutchings et al. (1988), along with the closer companions to the SSE and NNE and the extension to the south of the quasar nucleus.

*2130+099 (II Zw 136, UGC 11736, VV 190, KW 64)*

Radio-quiet [$z = 0.063$, $\log_{10}(L_{5\,\mathrm{GHz}}) = 21.45$]

The host of this low-redshift quasar resembles an inclined disc, and appears to have a large number of close or linked companions. The nearer of the two in the SE quadrant does not appear in previous optical images (Bothun et al. 1984; Gehren et al. 1984; Hutchings et al. 1984b; Smith et al. 1986; Hickson & Hutchings 1987). Several papers have drawn attention to a possible spiral structure in the host galaxy (Gehren et al. 1984; Hutchings et al. 1984a; Hickson & Hutchings 1987). These spiral features are most clearly seen in *B*-band images, so it is perhaps not surprising that they are not apparent in our *K*-band image. The linking luminosity to the SW companion is seen in all but the earliest optical images, whilst the connection to the more distant SE companion is only seen in Gehren et al. (1984). Spectra of the host galaxy have been obtained by Boroson et al. (1982) and also by Hickson & Hutchings (1987) (of the region thought to be a spiral arm). The results suggest that both early- and late-type stars are present. Condon, Gower & Hutchings (1987) claim to have detected radio-continuum emission from the stellar disc of the galaxy. Their 1.49-GHz map shows low-level emission in a 5-arcsec region centred on the quasar, with an extension in the same position angle as that of the major axis of the galaxy at *K*.

*2135−147 (PKS 2135−14, PHL 1657, OX−158, MSH 21−115)*

Radio-loud [$z = 0.200$, $\log_{10}(L_{5\,\mathrm{GHz}}) = 25.27$]

Stockton (1982) showed that the secondary nucleus and quasar are at the same redshift. Our image shows much more extended emission than has been seen previously. Both companions to the NW are also detected in the *V*-band image of Smith et al. (1986). Possible new features are the extended luminosity around the brighter of these, and the faint tail extending WSW of the quasar. We confirm the large area of nebulosity to the NNE which was detected by Hutchings et al. (1984). Hickson & Hutchings (1987) have carried out imaging spectroscopy of this source and comment, as did Stockton (1982), that the secondary nucleus may have an active spectrum. In the radio this quasar is an FRII source of diameter 160 arcsec, with a strong core (Gower & Hutchings 1984b).

*2141+175 (OX 169, MC3)*

Radio-loud [$z = 0.213$, $\log_{10}(L_{5\,\mathrm{GHz}}) = 24.81$]

We confirm the extension to the NW seen by Smith et al. (1986), and also note the filaments on the N and SE edge of the host galaxy. Two or possibly three compact objects are present NE of the quasar. The more northern two are not seen in previous studies. After removal of the PSF, the SE extension appears less jet-like, narrowing as it approaches the nucleus. Heckman et al. (1986) presented a *V*-band image showing the two thin extensions but also a 'fan-like' extension to the SW. This does not appear in our frame. The [O III] image shown in Heckman et al. (1986) has a sequence of faint knots south of the nucleus. Off-nuclear spectroscopy by Boroson & Oke (1984) showed that H$\alpha$ emission (and possibly also MgH absorption) is present along the SE extension, but no [O III] emission was detected. This object has recently been the subject of a detailed investigation by Stockton & Farnham (1991). They conclude that the luminosity of the thin extended structure is definitely produced by old stars, and is most probably an edge-on example of the sort of tidal-tail structure apparently seen face-on in 0157+001 and 3C48 (see Section 4.5). The quasar is a compact (< 4 arcsec), flat-spectrum radio source (Fiegelson, Isobe & Kembhavi 1984).

*2201+315 (4C 31.63, GC 2201+315, B2 2201+31A)*

Radio-loud [$z = 0.298$, $\log_{10}(L_{5\,\mathrm{GHz}}) = 25.76$]

This image was badly affected by ghosts. The extension to the NE is the remnant of a group of these after linear inter-

polation. The small companion 8 arcsec east of the nucleus lies in the same region as an extension seen by Gehren et al. (1984). The companions to the S, SW and WNW seen in our *K*-band image are also seen in their optical image. The surrounding nebulosity envelops the SW and NW companions in both frames. Hutchings et al. (1984) have also published an optical image of this quasar. It shows the two bright companions west of the nucleus, but not the fainter one to the south. They also noted the linking luminosity beween quasar and companions and some twisting of the outer isophotes. In the radio this quasar is an FRII source of diameter 90 arcsec, with a bright core (Gower & Hutchings 1984b; Neff & Brown 1984).

*2215−037 (EX 2215−037)*

Radio-quiet ($z = 0.241$)

The two main frames that make up this image had to be shifted by a significant fraction of the frame in order to align the quasar centroids. This has resulted in the loss of data in the bottom 4 arcsec of the image. In addition, the final image is the result of only 48 min of integration. The quasar appears to be connected to a large companion object, but Heckman et al. (1984) have measured the redshifts of both the quasar and the large companion and found a significant difference of 43 000 km $s^{-1}$. Possible extensions towards the SW companion and another compact companion 18 arcsec NW of the nucleus are also detected. Smith et al. (1986) have imaged this quasar, detecting all three companions and the apparent linking nebulosity between two of them. Hutchings et al. (1989) attribute "elliptical characteristics' to the host galaxy, but do not classify it as interacting.

*2247+140 (PKS 2247+14, 4C 14.82, OY 181)*

Radio-loud [$z = 0.237$, $\log_{10}(L_{5\,\mathrm{GHz}}) = 25.31$]

Early optical observations of this source (Gehren et al. 1984; Hutchings et al. 1984) did not reveal the bright companion to the SE of the quasar, but deep CCD imaging by Smith et al. (1986) and Hutchings et al. (1988) showed the companion and the NW/SE elongation of the host galaxy. The two companions to the SW and the one in the extreme SE of our image are also visible in the image by Smith et al. (1986), but the short tail-like extension from the SE of the host galaxy appears to be a previously undetected feature. The quasar is a steep-spectrum, compact radio source (van Breugel, Miley & Heckman 1984).

*2344+183*

Radio-quiet ($z = 0.138$)

Two faint extensions NW of this source are seen, and there is a bright extended 'blob' 16 arcsec SW of the nucleus. Hutchings et al. (1989) noted a bar-like feature suggestive of a spiral galaxy. This is not visible in our frame, although a slight WSW bulge is evident. Malkan et al. (1984) note the presence of several nearby galaxies, but these lie outside or on the perimeter of the IRCAM field of view.

*2349−014 (PG 2349−014, PKS 2349−01, PB 5564)*

Radio-loud [$z = 0.173$, $\log_{10}(L_{5\,\mathrm{GHz}}) = 24.86$]

A strong interaction appears to be occurring here and, to show this fully, the image has been presented with the quasar off-centre. A large companion galaxy and two smaller objects are seen SE of the quasar. All three are surrounded by extended luminosity. There is more faint, extended luminosity SW of the nucleus, but its structure appears complex. Véron-Cetty & Woltjer (1990) present an *i*-band image which seems to confirm the presence of the third companion (between the quasar and the galaxy), but their field of view does not extend far enough east to show the object SE of the interacting galaxy. In the radio this quasar is an FRII source of diameter 53 arcsec, with a strong core (Antonucci 1985).

*2355−082 (PKS 2355−082, PHL 6113)*

Radio-loud [$z = 0.211$, $\log_{10}(L_{5\,\mathrm{GHz}}) = 24.50$]

There are three obvious companions, the one in the SW corner being also visible in the optical image of Smith et al. (1986). The other two have not been detected before. At radio wavelengths this quasar is a small (5 arcsec) FRII source (Gower & Hutchings 1984b).

## 4 RESULTS AND DISCUSSION

### 4.1 Comparison of quasar hosts and radio galaxies

Although we do not, at present, possess similarly deep *K*-band images of a comparison sample of radio galaxies, a simple and direct comparison can be made between the *K* magnitudes of the quasar hosts and those predicted by the observationally determined *K*–*z* relation for radio galaxies (Lilly, Longair & Allington-Smith 1985; Dunlop et al. 1989). This comparison is appealingly model-independent, requiring neither luminosity profiles nor *k*-corrections to be assumed. However, it cannot be attempted without some knowledge of the extent to which the *K* luminosity of the quasar hosts has been underestimated due to complete subtraction of the PSF. To estimate the size of this correction, we investigated the impact of core subtraction on the *K* magnitude of the control radio galaxy PKS 1215−033 ($z = 0.184$). This experiment produced a magnitude shift of $\Delta K \simeq 0.75$ mag, with the 12-arcsec aperture magnitude increasing from $K = 14.38 \pm 0.05$ to $K = 15.11 \pm 0.25$ as a result of PSF subtraction from the centre of the galaxy.

For simplicity, we have therefore applied a 0.75-mag shift to the radio galaxy *K*–*z* relation before comparing it with the magnitudes of the quasars and their hosts. The result of this comparison is shown in Fig. 7, and it is clear that the quasar host galaxies display an extremely tight Hubble relation, consistent with that observed for powerful radio galaxies.

To illustrate more clearly the reduction in dispersion that has occurred, and to compare the *K* magnitudes of the RQQ and RLQ hosts, we show in Fig. 8 the distributions of residual *K* magnitude ($K_{\mathrm{res}}$) with respect to the *K* magnitude predicted from the radio galaxy *K*–*z* relation. For the sample as a whole, $\langle K_{\mathrm{res}} \rangle = -1.88$ prior to subtraction of the PSF, and $\langle K_{\mathrm{res}} \rangle = 0.028$ afterwards, while the scatter has been reduced from $\sigma_K = 0.62$ to $\sigma_K = 0.46$. This reduction in the scatter is reassuring, given the obvious introduction of error

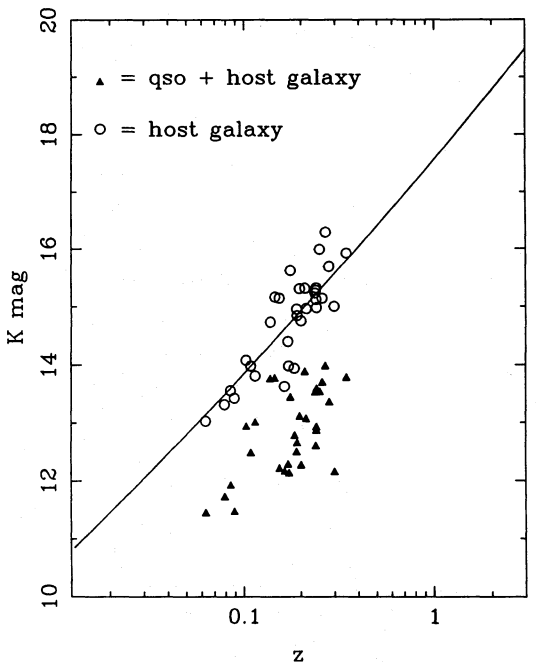


**Figure 7.** Positions of the quasars before and after subtraction of the nuclear component on the $K$–$z$ diagram. The line is the empirical fit to the $K$–$z$ relation for powerful radio galaxies (Lilly et al. 1985) shifted by 0.75 mag to correct for the systematic oversubtraction of the PSF (see Section 4.1). The quasar hosts clearly follow a Hubble relation very similar to that of powerful radio galaxies and thus, like radio galaxies, appear to be remarkably good standard candles at $K$.

during removal of the complex PSF. A similar pattern is seen within the individual RLQ and RQQ subsamples; for the RLQs, $\langle K_{res}\rangle = -2.05$ to $\langle K_{res}\rangle = 0.006$ and $\sigma_K = 0.60$ to $\sigma_K = 0.39$; for the RQQs, $\langle K_{res}\rangle = -1.76$ to $\langle K_{res}\rangle = 0.045$ and $\sigma_K = 0.62$ to $\sigma_K = 0.51$ (the four RQQs formally excluded from the sample comparison are included in Fig. 8, but all lie within the central bin).

These results mean that, in contrast to the findings of optical studies, we detect no evidence of any significant difference between the $K$ magnitudes of the RLQ and RQQ hosts. This result may, however, be consistent with the average magnitude difference found in the optical, since the reported size of this systematic difference decreases with increasing wavelength; $\Delta B = 1.9$ mag, $\Delta R = 1.3$ mag, $\Delta i = 0.6$ mag (Hutchings et al. 1989; Véron-Cetty & Woltjer 1990). Our null result may therefore indicate that the reported tendency for the hosts of RLQs to have bluer optical colours than their RQQ counterparts also extends to their optical–infrared colours. The systematic difference between the *optical* magnitudes of the two classes of host galaxy could therefore be regarded simply as a restatement of the fact that RLQ hosts are bluer, rather than indicating a difference in, for example, galaxy mass, but deep optical imaging of our matched quasar samples is required to confirm this.

Although simple, the 0.75-mag offset applied to the radio galaxy $K$–$z$ relation in Figs 7 and 8 is unlikely to be significantly in error for the present purpose of sample comparison. While we could attempt to incorporate some redshift dependence in the obvious sense, a more sophisticated correction also requires knowledge of the structures and scale-

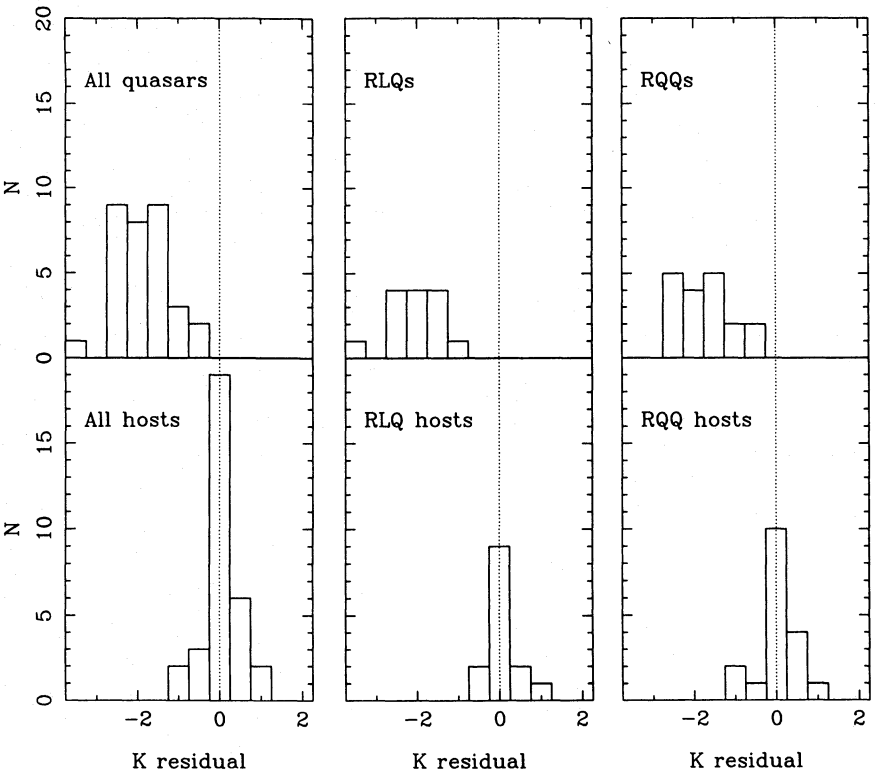


**Figure 8.** Histograms of observed magnitude residuals with respect to the $K$–$z$ relation shown in Fig. 7. These diagrams show clearly that, despite the inevitable introduction of errors as a result of PSF subtraction, the dispersion of the quasars is considerably greater than that of their hosts. In contrast to results at optical wavelengths, there is no evidence of any difference between the $K$ magnitudes of the hosts of RLQs and the hosts of RQQs.

lengths of both the quasar hosts and a comparison sample of radio galaxies; this is beyond the scope of this paper (see Section 4.5). We therefore conclude from the present data that there appears to be no significant difference between the average $K$ magnitudes of quasar hosts and powerful radio galaxies. In particular, like powerful radio galaxies, quasar host galaxies seem to be excellent standard candles at $K$. In fact, the remarkably low dispersion ($\sigma = 0.46$ mag) of the host galaxy magnitude distribution seen in the left-hand plot of Fig. 8 is actually smaller than that seen for radio galaxies (for 40 radio galaxies from the 1-Jy and 3CR samples in the redshift range $0.06 < z < 0.35$, $\sigma_K = 0.65$ mag), which leads one to speculate that the radio galaxy $K$–$z$ relation may be broadened by varying contributions from the active nuclei (see Section 4.5).

### 4.2 Absolute magnitudes

We have calculated absolute $K$ magnitudes, $M_K$, for the quasar host galaxies, using the $k$-corrections for first-ranked elliptical galaxies adopted by Neugebauer et al. (1985). The resulting values of $M_K$ for the hosts given in Table 2 include the 0.75-mag correction. The values of $M_K$ (qso-host) therefore represent the $K$-band luminosity that remains to be attributed to the active nucleus after removal of both the measured host galaxy flux and the 0.75-mag correction to that flux. These corrected values have then been used to calculate the $K$-band luminosity ratio for each source, $L_{\rm qso\text{-}host}:L_{\rm host}$, listed in the final column of Table 2.

The absolute magnitudes of the hosts are plotted against their redshifts in Fig. 9, along with the transformed radio galaxy $K$–$z$ relation. On this diagram, the effects of aperture corrections and $k$-corrections conspire to offset each other, producing a near-horizontal relation. Also shown for comparison are the absolute $K$ magnitudes of E/S0 and spiral members of the $z = 0.37$ cluster Abell 370 (Aragón-Salamanca, Ellis & Sharples 1991), corrected to a 12-arcsec diameter aperture. This diagram demonstrates that RLQs, RQQs and powerful radio galaxies reside *solely* in galaxies selected from the high-luminosity exponential tail of the $K$-band luminosity function (note that no selection bias can produce an artificial *lower* limit to the host galaxy luminosity), and that the scatter in $M_K$ displayed by the host galaxies is much smaller than that seen at optical wavelengths (e.g. see Figs 3 and 5 in Smith et al. 1986).

For the RQQs $\langle M_K \rangle = -25.7 \pm 0.57$, while for the RLQs $\langle M_K \rangle = -25.8 \pm 0.40$. It is interesting to compare these values with the corresponding figures for Brightest Cluster Members (BCM) given by Thuan & Puschell (1989), who find $\langle M_K \rangle_{\rm BCM} = -25.9 \pm 0.34$. The BCM $M_K$ values were determined through an aperture of diameter 32 kpc but, since (at the mean redshift of our quasar sample, $\langle z \rangle \simeq 0.2$) our aperture of 12-arcsec diameter corresponds to $\simeq 35$ kpc, our $M_K$ values can be reasonably compared. We therefore conclude that the hosts of both RLQs and RQQs are comparable to BCMs in both mean brightness and dispersion at $K$ (see Section 4.5 for discussion of the robustness of the 0.75-mag correction in this comparison).

Since there is no obvious selection effect that can give rise to a lower luminosity cut-off in the luminosity function of quasar host galaxies, Fig. 9 indicates that, for whatever reason, galaxies fainter than $M_K \simeq -25$ do not house quasars. This result is consistent with the conclusion reached at optical wavelengths by Véron-Cetty & Woltjer (1990) that galaxies with $M_V > -21$ have difficulty making quasars.

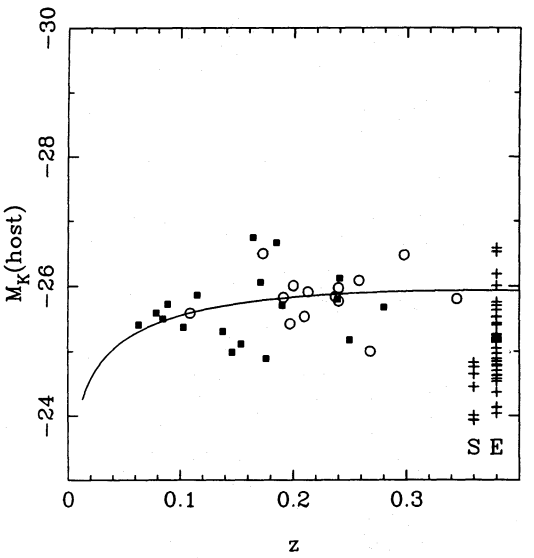


**Figure 9.** Absolute magnitudes of the RQQ hosts (squares) and the RLQ hosts (circles) plotted against redshift. $M_K$ has been calculated from the 12-arcsec aperture photometry, after addition of the 0.75-mag correction, and using the $k$-corrections for elliptical galaxies given by Neugebauer et al. (1985). The line is the transformed $K$–$z$ relation for radio galaxies from Fig. 7. Crosses indicate the absolute magnitudes (corrected to a 12-arcsec aperture) of spiral and E/S0 galaxies in the $z = 0.37$ cluster Abell 370 (Aragón-Salamanca et al. 1991).

There remains only a weak correlation between host galaxy luminosity and quasar luminosity after subtraction of the corrected host galaxy flux from the quasar. This is shown in Fig. 10 for the two matched 14-object samples. Calculation of the Spearman rank correlation coefficient yields a value of $r_s = 0.32$ ($p = 0.05$) for the full 28-source sample, which is in fact the consequence of a significant correlation in the RLQ sample ($r_s = 0.57$; $p \simeq 0.02$) combined with a null result for the RQQ sample ($r_s = 0.095$; $p > 0.2$). Comparison with the results at optical wavelengths is hampered by disagreements between different studies. For example, Hutchings et al. (1984) found a strong correlation between $L_{\rm host}$ and $L_{\rm qso}$ at optical wavelengths, reported to extend to $H$ (1.65 μm) by Neugebauer et al. (1985). Smith et al. (1986) and Véron-Cetty & Woltjer (1990) find a much weaker correlation and cast doubt on its reality, pointing out that it is due, at least in part, to the fact that weaker nuclei in bright hosts are selectively excluded from quasar samples. In addition, different definitions of $L_{\rm qso}$ can affect the correlation; attribution of all the central flux to the quasar (e.g. Hutchings et al. 1984) will inevitably lead to some coupling between the derived quasar and galaxy luminosities. The weak correlation seen at $K$ certainly appears to have a shallower slope than that which has been claimed in the optical, a result that again is probably another manifestation of the improved 'standard-candle' behaviour displayed by the host galaxies at $K$.

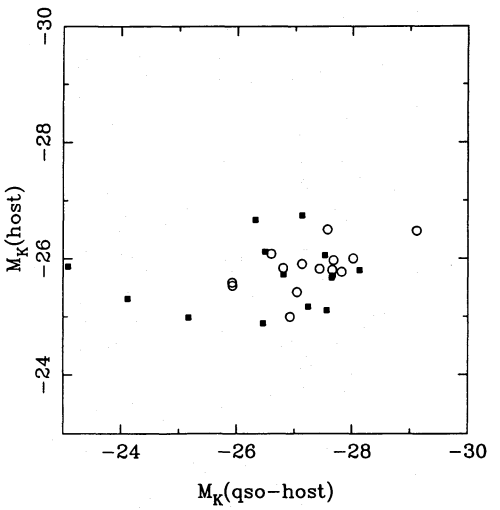


**Figure 10.** Host-galaxy absolute magnitude $M_K$ plotted against quasar $M_K$ for the RQQs (squares) and RLQs (circles). The quasar luminosity has been taken to be that which remains after subtraction of the host-galaxy flux and the central correction.

### 4.3 Axial ratios, sizes and position angles

To determine the axial ratios of the host galaxies in an objective manner, we employed a moment analysis (this technique also provides an objective and quantitative method of identifying structural features such as spiral arms or tidal tails). The centroid of the image was determined by calculating the first (flux-weighted) moments of the image $\langle x \rangle$ and $\langle y \rangle$. The second moments $\langle x^2 \rangle$, $\langle y^2 \rangle$ and $\langle xy \rangle$ were then calculated about the mean position, with diagonalization of the resulting symmetric matrix of second moments yielding the position angle of the major axis of the galaxy. The extent of ellipticity was then parametrized via the axial ratio $b/a = (\langle y^2 \rangle / \langle x^2 \rangle)^{1/2}$. Pixel participation in this calculation was limited to $\mu_K < 21.5$ mag arcsec$^{-2}$, and to those within a chosen radius of the galaxy centroid. To allow the structure of the entire host galaxy to be quantified, the analysis was repeatedly performed as the chosen aperture radius was steadily increased from zero to 15 arcsec.

In Fig. 11 we show the resulting variation of position angle and axial ratio with radius for two objects (both radio-quiet), −0007+106 and 0157+001. These are the only two

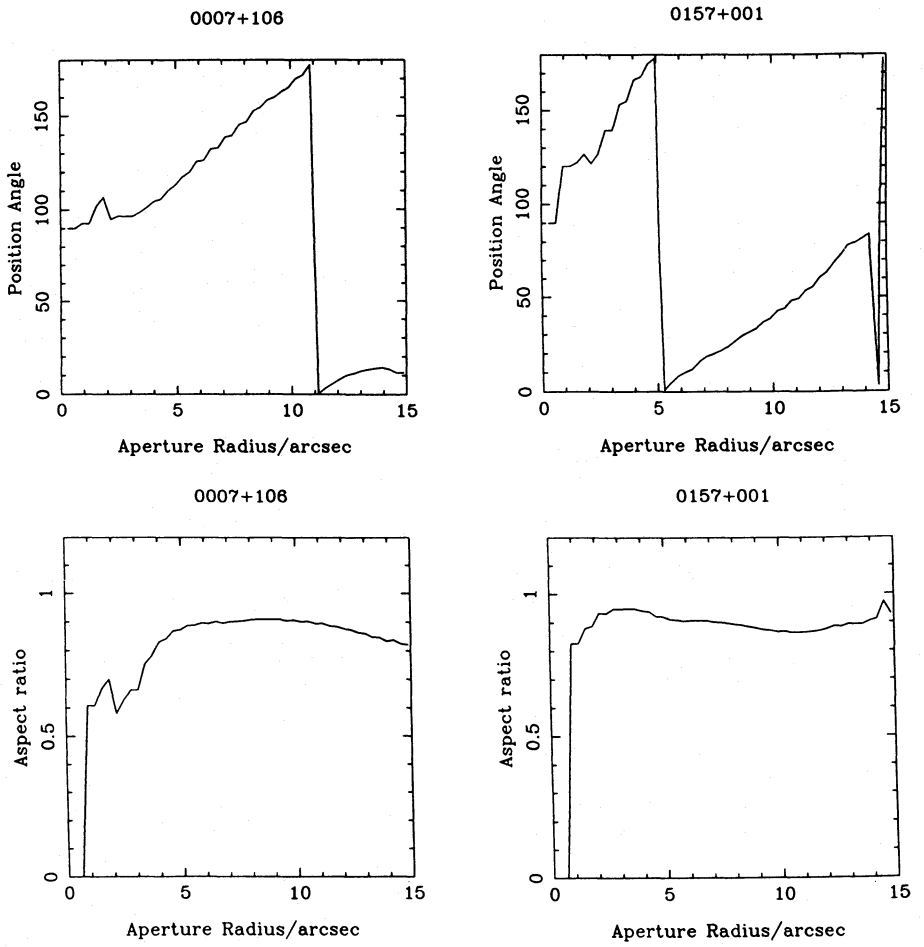


**Figure 11.** Radial dependence of position angle and axial ratio $b/a$ for the two radio-quiet quasars 0007+106 and 0157+001 according to the moment analysis described in Section 4.3.

quasar host galaxies in the sample that display a steady and smooth rotation of position angle over a large range of radii, indicative of either spiral structure or tidal tails. The interpretation of the isophote rotation displayed by 0157+001 is discussed further in Section 4.5

Comparison of the axial ratios of RLQ and RQQ hosts was performed by confining attention to those galaxies whose axial ratios changed by less than $\Delta(b/a)=0.1$ between a radius of 10 arcsec and the final radius of 15 arcsec. This was necessary to exclude galaxies whose axial ratio was strongly affected by bright companions. The axial ratios of the remaining 12 RLQ hosts and 11 RQQ hosts were then taken to be the average of the axial ratios calculated at 10- and 15-arcsec radius. The resulting distributions are shown in Fig. 12. The distributions have very similar means ($\langle b/a\rangle_{RQQ}=0.78$, $\langle b/a\rangle_{RLQ}=0.77$), but the RQQ distribution is noticeably broader ($\sigma_{RQQ}=0.17$; $\sigma_{RLQ}=0.09$). This is obviously suggestive of RQQs residing in disc galaxies with a range of orientations, while the asymmetric shape of the RLQ distribution peaking at $b/a>0.8$ is expected under the elliptical host hypothesis (Sandage, Freeman & Stokes 1970). The statistics are poor, however, and use of the KS statistic shows that formally the two distributions differ only at the $1.5\sigma$ level.

What is obvious is the lack of host galaxies with $b/a<0.5$; if a significant number of the hosts are disc galaxies, then there is a deficiency of edge-on galaxies in comparison to the known $b/a$ distributions for spiral or S0 galaxies which are virtually flat (Sandage et al. 1970). A similar deficiency of edge-on discs is apparent in optical studies of quasar hosts and, as noted by Malkan et al. (1984), the axial ratio distribution for radio-quiet hosts is most similar to that for Seyfert 1 galaxies (Keel 1980), which are known to be discs. There thus appears to be a selection bias against finding active nuclei in an edge-on disc (presumably due to dust obscuration), consistent with other recent evidence of anisotropic emission (e.g. Tadhunter & Tsvetanov 1989), and this will tend to reduce the potential diagnostic power of comparison of axial ratio distributions. Thus, although not significantly different, the axial ratio distributions shown in Fig. 12 are, in fact, consistent with the RLQ = elliptical-host, RQQ-spiral-host hypothesis.

In Fig. 13, we compare the host-galaxy size distributions of the matched samples of radio-loud and radio-quiet quasars. Major- and minor-axis dimensions were determined from the $\mu_K=21.5$ mag arcsec$^{-2}$ isophote in each image. On average, the host galaxies of RLQs are slightly larger than their radio-quiet counterparts, but the difference is not very significant: for the major axis $\langle RLQ\rangle=94$ kpc, $\langle RQQ\rangle=75$ kpc, while for the minor axes $\langle RLQ\rangle=68$ kpc, $\langle RQQ\rangle=54$ kpc. Both samples display a clear redshift-independent minimum dimension of $\simeq 40$ kpc. Interestingly, the radio galaxy PKS 1215−033 is 50 kpc in both dimensions, placing it at the bottom end of the distributions shown in Fig. 13. A detailed comparison of the dimensions and morphologies of quasar hosts and radio *galaxies* at $K$ will be the subject of a subsequent paper.

Finally, for the radio-loud quasars, it is of interest to compare the position angles (PAs) derived from our $K$-band images with the position angles of the radio sources, to check whether there is any evidence of alignment between the radio structure and the host galaxy. Of the 14 radio-loud quasars in our sample, six are 'compact' radio sources (<5 arcsec) in the sense that they are not extended on scales comparable to the infrared host-galaxy emission. In Fig. 14 we show the distribution of $\Delta PA$(radio − IR) ($K$-band PAs determined from the moment analysis at a radius of 8 arcsec; see references in Section 3.5 for radio maps) for the remaining sample of eight RLQs. There is tentative evidence of an alignment effect, but the sample is really too small to draw any definite

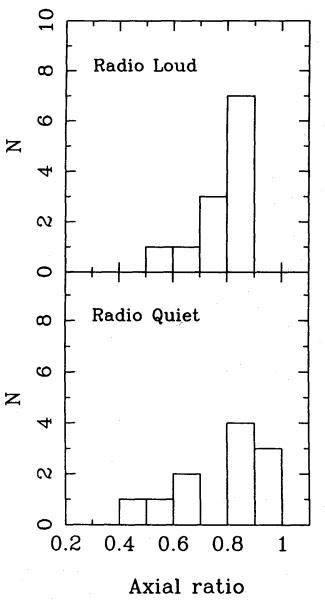


**Figure 12.** Comparison of the distributions of axial ratio for the 12 RLQ and 11 RQQ hosts for which $b/a$ differs by less than 0.1 between radii of 10 and 15 arcsec.

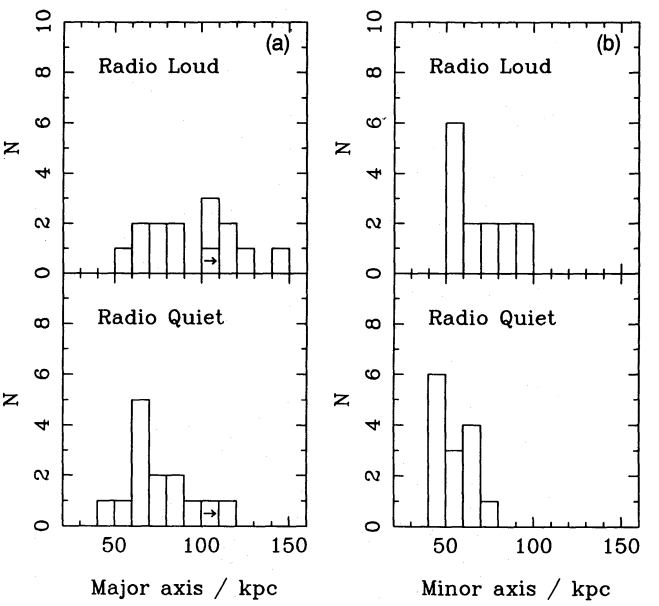


**Figure 13.** Comparison of distributions of RLQ and RQQ host-galaxy size determined from the $\mu_K=21.5$ mag arcsec$^{-2}$ isophote: (a) major axis, (b) minor axis.

conclusions. Formally, comparison with an isotropic distribution using the KS test yields $R_{max} = 0.325$ at 25°, giving a significance level of $p = 0.275$. Clearly, if any alignment effect is present, it is at a low level and is certainly not comparable to the dramatic alignments seen at $z \simeq 1$ in some 3CR radio galaxies. However, this is perhaps not unexpected, since (i) the alignments seen in high-redshift radio galaxies are most prominent in the rest-frame optical–UV, and (ii) the low-redshift RLQs investigated here are less radio luminous than the 3CR sources at $z \simeq 1$, but are in fact better compared with, for example, the Parkes Selected Regions radio galaxies at $z \simeq 1$ which also display no significant alignment effect in the near-IR (Dunlop & Peacock 1993).

### 4.4 Companions

One of the most striking features in our $K$-band images is the essentially universal incidence of possible 'companion' objects, despite the small size ($36 \times 38$ arcsec$^2$) of the IRCAM field of view. A detailed statistical analysis of these 'companions' will be presented elsewhere, but some basic conclusions can readily be drawn from the data presented in Table 3.

Table 3 gives positions and $K$ magnitudes of all 'companion' objects for which magnitudes could be reliably determined ($\sigma_{mag} < 0.5$) through an aperture of 5-arcsec diameter. Given the depth and homogeneity of the imaging data, we are confident that this 'companion survey' is effectively complete to $K \simeq 19$.

Considering the two 14-source matched RLQ and RQQ samples, we find that, with the single exception of 1004+130 (for which the image is badly contaminated by scattered light), *all* the quasar hosts have at least one 'companion' object. Thus all the quasars in the sample have at least one apparent companion source within a projected radius of 100 kpc. In Fig. 15, we show, for the two samples, a plot of projected distance to nearest companion (simply assuming the same redshift as the quasar) versus quasar redshift. As can be seen from this diagram, eight RLQs and nine RQQs have an apparent 'companion' within a projected radius of 50 kpc. There is no significant difference between the two samples: the average projected radius to the nearest companion is $50 \pm 17$ kpc for the radio-loud sample, and $43 \pm 13$ kpc for the radio-quiets. It is, of course, possible that this similarity simply reflects the fact that many (or possibly most) of the apparent companions are in fact background/foreground sources not physically associated with the quasar host galaxy. To investigate whether there exists any evidence for an excess of companion objects, we next consider the $K$-band number counts derived from our images.

Again considering only the matched samples (and excluding 1004+130 from the RLQ sample), a total of 35 RLQ 'companions' and 44 RQQ 'companions' with $K < 19$ appear in our 'survey'. These numbers translate into integrated number counts of $2.7 \times 10^4$ and $3.1 \times 10^4$ deg$^{-2}$ respectively. These figures do not differ significantly from each other, but are a *factor of 2* higher than the integrated number count to $K = 19$ of $1.5 \times 10^4$ deg$^{-2}$ given by Cowie et al. (1990) (prior to star-galaxy separation). In Fig. 16 we compare the differential $K$-band number counts derived from our RLQ and RQQ surveys with that observed in the field (Cowie et al. 1990; Glazebrook et al. 1991). An obvious and interesting

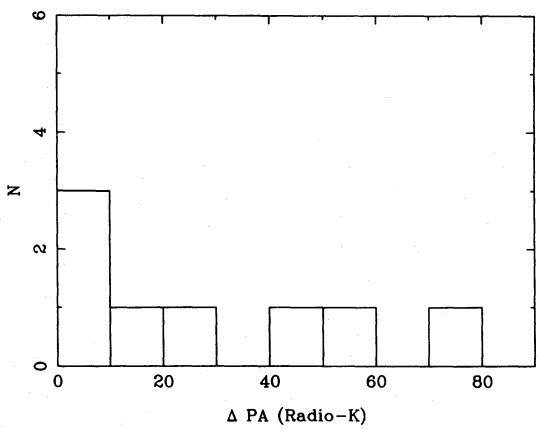


**Figure 14.** The distribution of $\Delta PA$ (radio $-$ $K$) for the eight RLQs with large-scale ($> 5$ arcsec) radio structure. $K$-band position angles were determined using the moment analysis described in Section 4.3, while radio position angles were obtained from maps for which references are given in Section 3.5.

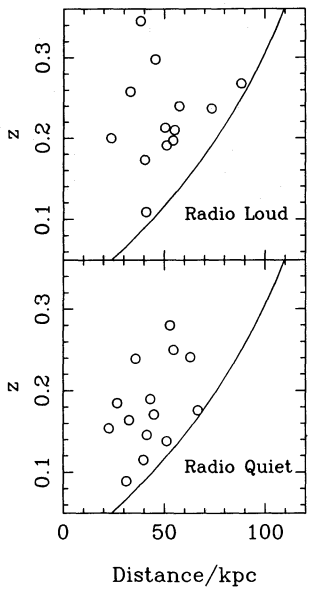


**Figure 15.** Redshift versus projected separation between each quasar and its nearest 'companion' object (assuming that the companion lies at the same redshift as the quasar) for the matched RLQ and RQQ samples. The curve indicates the redshift dependence of a fixed angular radius of 18 arcsec, which is the typical distance between the quasar nucleus and the nearest edge of the IRCAM frame.

feature of this diagram is that the number counts within the bin $18 < K < 19$ from the RLQ and RQQ surveys ($1.15 \times 10^4$ and $1.07 \times 10^4$ deg$^{-2}$ respectively), in addition to being essentially identical to each other, are also remarkably consistent with that expected from the field-galaxy number counts. It is clear, therefore, that the origin of any excess in our integrated number counts is *not* to be found in the fainter ($K > 18$) apparent companions, and that the high incidence of these faint sources is in fact consistent with the expected background number counts at these magnitudes. This, in

turn, implies that very few of the apparent companions with $K > 18$ are likely to be genuine physical companions of the quasars.

As can be seen in Fig. 16, the origin of any 'companion excess' is therefore to be found at brighter apparent magnitudes ($K < 18$). The statistics in the brightest bins are inevitably poor, but at $K \simeq 17$–$18$ the surface density of apparent companions for both RLQ and RQQ samples is higher than the predicted background galaxy count by a factor $\simeq 2.5$ (essentially our number counts at $K \simeq 17.5$ are the same as at $K \simeq 18.5$). Since detailed star-galaxy separation is beyond the scope of this paper and we lack control fields of comparable depth, this apparent excess at brighter magnitudes should be treated with caution. Nevertheless, the raw counts from the bright $K$-band survey of Glazebrook et al. (1991) yield an integrated surface density of 2800 objects deg$^{-2}$ down to $K = 17.5$, prior to stellar decontamination. The corresponding number counts derived from our RLQ and RQQ samples are 9200 and 15 000 respectively. These numbers provide preliminary evidence of a significant excess of galaxies around both classes of quasar, but also indicate a possible difference between the two samples. In fact, in the magnitude range $K = 16$–$17.5$ there are 15 RQQ companions compared to only eight RLQ companions – i.e. at $K \simeq 17$ the surface density of apparent companions around RQQs is approximately twice that found around RLQs. This preliminary result appears to support the tentative conclusion reached by Yee (1987) that actual interaction with other galaxies (rather than the ambient physical conditions of a higher-galaxy-density region) could be more important in the triggering of RQQs than RLQs.

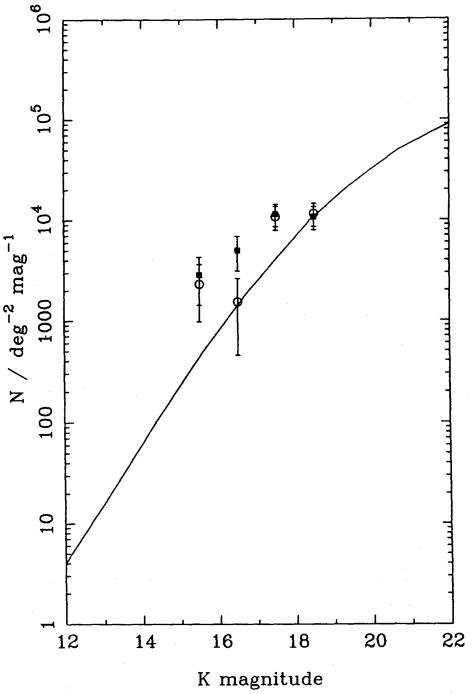


**Figure 16.** Comparison of $K$-band number counts derived from the RLQ (open circles) and RQQ (filled squares) imaging 'surveys' with the predicted field-galaxy number counts derived from the $K$-band surveys of Cowie et al. (1990) and Glazebrook et al. (1991).

Finally, in Fig. 17, we present a revised plot of projected distance to nearest companion after rejecting all companions with $K > 18$. Comparison with Fig. 15 shows that the number of very close companions (separation $< 40$ kpc) has been relatively unaffected by removal of the faint companions from the candidate list; the main effect of this change is the removal of five RLQs and three RQQs which have no companions with $K < 18$ within 18 arcsec of the source. Excluding these upper limits, the revised mean projected distance to the nearest companion is 54 kpc for the RLQs and 49 kpc for the RQQs – i.e. essentially unchanged and still clearly consistent with each other. The redshift independence apparent in Fig. 17 lends credence to the suggestion that many of these sources are actual physical companions rather than chance projections. However, whereas in Fig. 15 11 out of the 13 RLQs (85 per cent) and 12 out of the 14 RQQs (86 per cent) have a companion within $\simeq 65$ kpc, the frequency has now dropped to 6 (46 per cent) and 11 (79 per cent) respectively (consistent with the difference in number counts around $K = 17$ discussed above).

### 4.5 Luminosity profiles – the example of 0157 + 001

The luminosity profiles derived from the images presented here will be analysed in a separate paper (Taylor et al., in preparation). As an illustrative example, we show in Fig. 18 the $K$-band luminosity profile of 0157 + 001, along with the results of attempting to model this quasar as a combination of a point-like nucleus and either a disc-like (Fig. 18a) or spheroidal (Fig. 18b) host galaxy. The conclusion of this modelling is that the host of 0.157 + 001 is best described as a spheroid of scalelength $r_e = 26.6 \pm 0.4$ kpc ($\chi^2_\nu = 1.29$). The fit for an exponential disc is somewhat less good ($\chi^2_\nu = 3.42$), and the derived scalelength of $r_0 = 12.7 \pm 0.4$ kpc is considerably smaller than the value of $r_0 = 20.7 \pm 1.0$ kpc derived by Smith et al. (1986) from their $V$-band image of this source

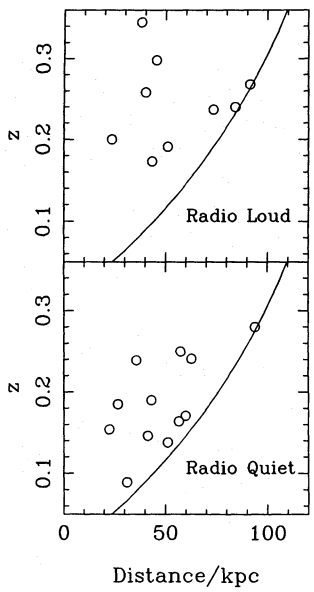


**Figure 17.** Revised version of Fig. 15 after rejection of sources with $K > 18$ from the list of apparent 'companions'.

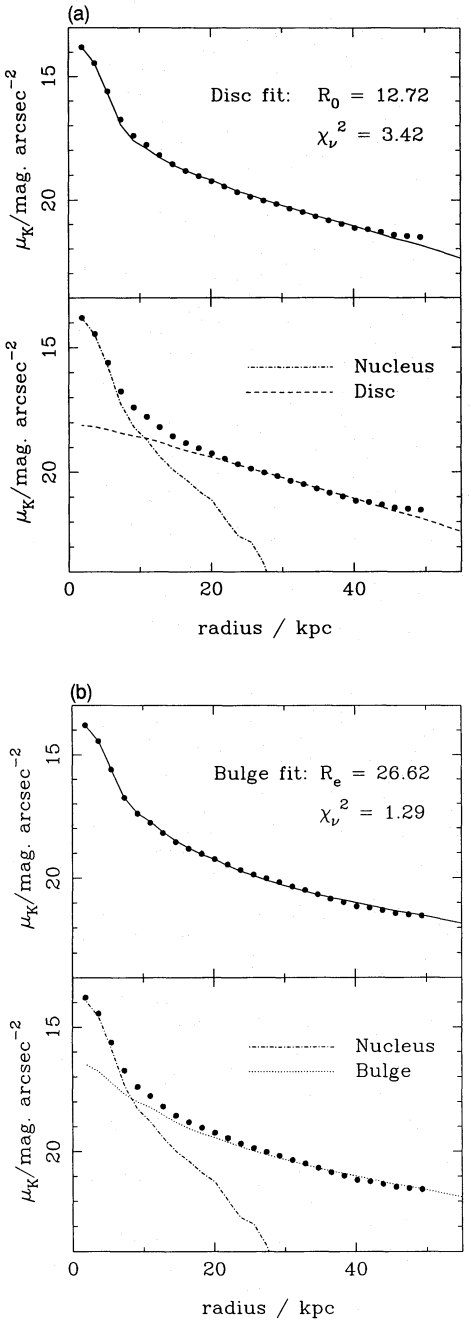


**Figure 18.** Modelling of the *K*-band luminosity profile of the radio-quiet quasar 0157+001 in terms of (a) stellar nucleus plus exponential disc host galaxy, (b) stellar nucleus plus spheroidal host galaxy. A spheroidal host products a better fit, in contrast to the result reported by Smith et al. (1986) that the *V*-band luminosity profile was only consistent with a disc-like host.

(after correcting to our cosmology). Although the preference displayed by our data for a spheroidal host is slight (and we would not wish to rule out the possibility of a disc host at this stage), this preference is unchanged by altering either the adopted background level or the choice of PSF representation from the ensemble of candidate stars. What is significant is that a spheroidal host can describe the *K*-band data successfully, whereas Smith et al. (1986) were unable to achieve a successful fit to their *V*-band luminosity profile using a de Vaucouleurs $r^{1/4}$ law.

Although it might be tempting to dismiss this disagreement (given, for example, the difficulties experienced in determining the IRCAM PSF), there is considerable supporting evidence that the galaxy is genuinely different in appearance at *K* as compared with *V*. In particular, there is a clear change in isophotal shape between *V* and *K*. In the *V*-band image of Smith et al. the galaxy appears quite elongated, and indeed Smith et al. found that an axial ratio of 0.6 (in position angle 80°) yielded the best galaxy model fit. In contrast, the isophotes are clearly much rounder at *K*, the moment analysis yielding an axial ratio of $\simeq 0.9$ over a wide range of radii (see Fig. 11). Two reasons can be identified for this change in shape. First, the arm-like feature to the north-east is undoubtedly bluer than the rest of the host galaxy; it is obviously much more prominent in the *V*-band image of Smith et al. than in our *K*-band image, and this waveband dependence is confirmed by MacKenty & Stockton (1984), who noted that the feature was less prominent in their *r*-band image than in their corresponding blue image (~3500–4800 Å). Secondly, both the *V*-band image of Smith et al. and the Cousin's *R*-band image of MacKenty & Stockton will contain contributions from redshifted [O III]5007-Å emission, which, as shown by Stockton & MacKenty (1987), is extended along a position angle of ~80°. This, then, appears to be an excellent example of how near-infrared imaging can reveal the structure of the underlying host galaxy, relatively uncontaminated by either emission-line gas or young stars associated with the nuclear activity and/or associated interactions.

Since 0157+001 is an RQQ according to our radio-power classification, our tentative conclusion that its host is, in fact, a giant elliptical galaxy conflicts with any simple-minded picture that all RQQs are housed in disc-like galaxies, while all RLQs have spheroidal hosts. A disc-like host has also been anticipated a priori by several authors on account of (i) the low axial ratio $b/a = 0.6$ seen at *V* (suggestive of an inclined disc; Smith et al. 1986), and (ii) the clearly detected spiral arm-like feature, which led to the smooth isophote rotation detected by the moment analysis (see Fig. 11). As discussed above, however, at *K* there is no longer any evidence to support the inclined-disc interpretation (the galaxy being essentially round), and tidal tails can also produce smooth rotation of the galaxy isophotes. In fact, as we show in Fig. 19, tidal disruption is almost certainly the cause of the apparent spiral structure seen in the host galaxy of 0157+001. Fig. 19 shows the result of subtracting an azimuthally median-averaged model galaxy from our *K*-band image of 0157+001. The remaining structure appears to be a clear tidal tail, linking the nucleus to a compact companion galaxy.

If the underlying host of 0157+001 is indeed spheroidal, then the derived de Vaucouleurs scalelength of $r_e = 27$ kpc is large but not unreasonable. For example, Owen & Laing (1989) found the hosts of 'twin-jet' (FR I) radio sources to have an average scalelength $r_e = 21$ kpc (when converted to $H_0 = 50$ km s$^{-1}$ Mpc$^{-1}$), and concluded that they could generally be described as D or cD galaxies.

This result for 0157+001 does not, of course, imply that all the hosts of RQQs are giant ellipticals, although it is interesting that a recent study of the environment of the RQQ

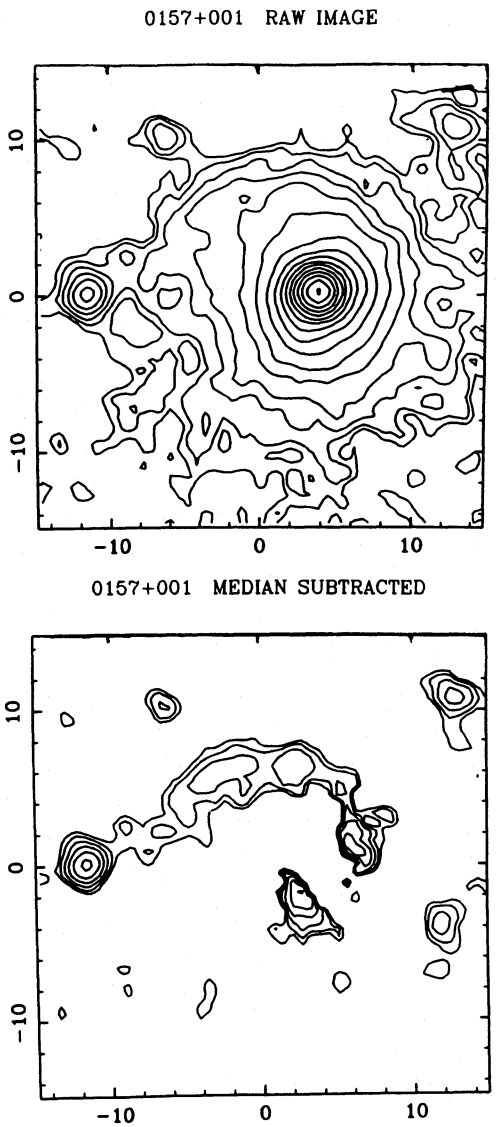


**Figure 19.** The *K*-band image of the RQQ 0157+001 before and after subtraction of an azimuthally median-averaged model galaxy. The residual image shows a clear tidal tail connecting the quasar nucleus to a compact companion galaxy, thus indicating that the smooth rotation of the isophotes seen in Fig. 11 should not be interpreted as evidence of spiral structure.

E1821+647 indicates that it also appears to be a cD galaxy at the centre of a rich cluster (Lacy, Rawlings & Hill 1992). Indeed, if one were to attempt RQQ/RLQ classification on the basis of radio structure rather than radio luminosity, then 0157+001 might be classified as radio-loud since, although weak, it does possess a core-jet radio structure reminiscent of radio-loud quasars (Miller & Rawlings, private communication), in contrast to other RQQs, such as 2130+099, whose diffuse extended radio structure can be explained as arising from supernova remnants distributed throughout the host galaxy (Condon et al. 1987). Whether the apparent preference displayed by 0157+001 for a spheroidal host applies to all RQQs (and indeed all RLQs) will be discussed in detail by Taylor et al. (1993).

Finally, this modelling of 0157+001 allows us to make a preliminary investigation of the validity of the 0.75-mag correction applied to the quasar hosts in Section 4.1. The modelling yields luminosity ratios $L_{\rm nuc}/L_{\rm host}$ (within a 12-arcsec aperture) of 2.1 and 3.4 for the spheroidal and disc galaxy models respectively, as compared to the value of 1.42 quoted in Table 2, indicating that for this particular object the magnitude correction of 0.75 mag (to account for over-subtraction of the nucleus) is a significant overestimate. In fact, the synthesized apparent magnitude of the best-fitting spheroidal model galaxy is $K=13.3$, while the exponential disc model has a magnitude of $K=13.6$ (as compared to the value of $K=12.9$ produced by subtracting 0.75 mag from the raw nuclear-subtracted value given in Table 2).

At first sight these numbers suggest that our global use of the 0.75-mag correction in the earlier analyses was not only crude, but also systematically in error. Modelling of the radio galaxy PKS 1215−033 provides reassurance that this is not the case, however, and indicates the likely origin of the discrepancy. The model that provides the best fit to the radio galaxy 1215−033 is a spheroid with scalelength $r_{\rm e}=17$ kpc (as anticipated, a disc model is strongly excluded for this object). There is also a non-negligible nuclear contribution in the model, the result being that the spheroidal galaxy has a synthesized apparent magnitude of $K=14.8$, as compared to the observed magnitude of $K=14.38$. This indicates that the 0.75-mag correction (which was derived from this object) consists of $\simeq 0.35$ mag to correct for the flux oversubtracted from the centre of the spheroidal galaxy, plus a further $\simeq 0.4$ mag to correct for a small nuclear component in the radio galaxy (either due to a bright galaxy nucleus, or a small AGN contribution).

We conclude, therefore, that the adoption of the simple 0.75-mag correction in the comparison of the *K* magnitudes of quasar hosts and radio galaxies remains valid. To a certain extent, at least for this particular comparison, the exact origin of this correction is unimportant; our initial modelling simply indicates that at least some (and perhaps all) radio galaxies contain a small nuclear contribution at *K*. An improved comparison requires detailed modelling of a control sample of radio galaxies as well as the quasars, in order to determine the exact level of nuclear contribution in every source; we are currently undertaking just such a study.

The validity of the 0.75-mag correction in the comparison of the absolute *K* magnitudes of the quasar hosts with those of BCMs (see Section 4.2) should be regarded with more caution, since we do not possess any control images with which to test whether the central *K*-band luminosities of BCMs are also in excess of that predicted by a pure de Vaucouleurs fit to their luminosity profiles. Obviously, the nature of the 0.75-mag correction becomes more important in the comparison of active and inactive galaxies, given the lack of any a priori evidence for nuclear activity in the latter. Nevertheless, even if the 0.75-mag correction is reduced to 0.35 mag (i.e. excluding the contribution of any nuclear component), the average absolute *K* magnitudes of both classes of quasar host will remain consistent with those of BCMs within the errors (see Section 4.2). As with the radio galaxies, an improvement in this comparison requires detailed modelling of the infrared morphologies of a control sample of BCMs.

These modelling results also indicate that, *if the bulk of the radio-quiet hosts are, in fact, disc galaxies*, then our conclusion that there is no significant difference between the *K*-band

luminosities of the hosts of RQQs and RLQs may have to be revised, but only slightly. Typically, as demonstrated by 0157+001, a disc model yields a host galaxy magnitude $\simeq 0.3$ mag fainter than a spheroidal model. Thus, even if all the radio-quiet hosts are discs, this model-dependent difference of 0.3 mag is still considerably smaller than the magnitude differences claimed in the optical. We re-emphasize that there is as yet no evidence at $K$ (or at $i$) to support the RQQ ≡ disc galaxy, RLQ ≡ elliptical hypothesis (and the initial modelling of 0157+001 provides evidence to the contrary).

## 5 CONCLUSIONS

We have assembled a data base of deep $K$-band images of matched samples of radio-loud and radio-quiet quasars at $z \simeq 0.2$. We have also devised an empirical method of point-spread-function determination which enables detailed modelling of the images presented here to be undertaken. The results of this modelling will be presented by Taylor et al. (in preparation), but a preliminary model-independent analysis of our images leads to the following conclusions.

(i) There is no evidence of any significant difference between the $K$-band luminosities of the hosts of RLQs and the hosts of RQQs.

(ii) The hosts of both classes of quasar appear to be good 'standard candles' at $K$, displaying a $K$–$z$ relation essentially identical to that already established for radio galaxies. Quasar hosts appear to be selected solely from the top of the $K$-band luminosity function.

(iii) A moment analysis of our images has yielded evidence for possible spiral structure in only two quasar hosts, and in at least one of these there is strong evidence that the detected smooth isophote rotation is actually due to tidal interaction with a companion galaxy.

(iv) The axial ratio distributions of the two classes of quasar host do not differ significantly, but are also consistent with the RQQ ≡ disc-host, RLQ ≡ spheroidal-host picture, given the known paucity of edge-on discs in active galaxy samples.

(v) There is weak evidence that the hosts of RLQs are on average somewhat larger than their radio-quiet counterparts. All the quasar hosts are large galaxies with minor-axis dimensions $> 40$ kpc.

(vi) There is only weak evidence for a low-redshift analogue of the alignment effect within the small subset of extended radio quasars included in our sample.

(vii) A preliminary analysis of the frequency of companion objects indicates that the incidence of faint objects with $K > 18$ is consistent with that expected from field galaxy counts in deep infrared surveys, but there is evidence for a significant excess of companions at brighter magnitudes.

(viii) Modelling of our $K$-band luminosity profile of the radio-quiet quasar 0157+001 favours a spheroidal host, rather than the disc-like host favoured by the $V$-band profile obtained by Smith et al. (1986). Its dimensions and absolute magnitude are consistent with a cD galaxy.

## ACKNOWLEDGMENTS

UKIRT is operated by the Royal Observatory Edinburgh on behalf of SERC. We thank the support staff for the first-rate assistance we received at the telescope, and in particular Colin Aspin for advice on data reduction. We gratefully acknowledge SERC for funding of the University of Central Lancashire minor node of STARLINK and for provision of travel funds. GLT is supported by a Research Studentship from the University of Central Lancashire.

## REFERENCES

Antonucci R. R. J., 1985, ApJS, 59, 499
Aragón-Salamanca A., Ellis R. S., Sharples R. M., 1991, MNRAS, 248, 128
Barthel P. D., 1989, ApJ, 336, 606
Barvainis R., 1990, ApJ, 353, 419
Bennett C. L., Lawrence C. R., Burke B. F., Hewitt J. N., Mahoney J., 1986, ApJS, 61, 1
Berriman G., Schmidt G. D., West S. C., Stockman H. S., 1990, ApJS, 74, 869
Boroson T. A., Oke J. B., 1984, ApJ, 281, 535
Boroson T. A., Oke J. B., Green R. F., 1982, ApJ, 263, 32
Boroson T. A., Persson S. E., Oke J. B., 1985, ApJ, 293, 120
Bothun G. D., Heckman T. M., Schommer R. A., Balick B., 1984, AJ, 89, 1293
Chini R., Kreysa E., Biermann P. L., 1989, A&A, 219, 87
Condon J. J., Gower A. C., Hutchings J. B., 1987, AJ, 93, 255
Cowie L. L., Gardner J. P., Lilly S. J., McLean I., 1990, ApJ, 360, L1
de Kool M., Begelman M. C., 1989, Nat, 338, 484
Dunlop J. S., Peacock J. A., 1990, MNRAS, 247, 19
Dunlop J. S., Peacock J. A., 1993, MNRAS, 263, 936
Dunlop J. S., Peacock J. A., Savage A., Lilly S. J., Heasley J. N., Simon A. J. B., 1989, MNRAS, 238, 1171
Ellingson E., Yee H. K. C., Green R. F., 1991, ApJ, 371, 49
Feigelson E. D., Isobe T., Kembhavi A., 1984, AJ, 89, 1464
Gehren T., Fried J., Wehinger P. A., Wyckoff S., 1984, ApJ, 278, 11
Glazebrook K., Peacock J. A., Miller L., Collins C. A., 1991, in Blanchard A. et al., eds, Physical Cosmology. Editions Frontières, Gif-sur-Yvette, p. 460
Gower A. C., Hutchings J. B., 1984a, PASP, 96, 19
Gower A. C., Hutchings J. B., 1984b, AJ, 89, 1658
Green R. F., Yee H. K. C., 1984, ApJS, 54, 495
Green R. F., Williams T B., Morton D. C., 1978, ApJ, 226, 729
Gregory P. C., Condon J. J., 1991, ApJS, 75, 1011
Heckman T. M., Bothun G. D., Balick B., Smith E. P., 1984, ApJ, 89, 958
Heckman T. M., Smith E. P., Baum S. A., van Breugel W. J. M., Miley G. K., Illingworth G. D., Bothun G. D., Balick B., 1986, ApJ, 311, 526
Hickson P., Hutchings J. B., 1987, ApJ, 312, 518
Hughes D. H., Robson E. I., Dunlop J. S., Gear W. K., 1993, MNRAS, 263, 607
Hutchings J. B., 1987, ApJ, 320, 122
Hutchings J. B., Crampton D., 1990, AJ, 99, 37
Hutchings J. B., McClure R. D., 1990, PASP, 102, 48
Hutchings J. B., Crampton D., Campbell B., 1984a, ApJ, 280, 41
Hutchings J. B., Crampton D.. Campbell B., Duncan D., Glendenning B., 1984b, ApJS, 55, 319
Hutchings J. B., Johnson I., Pyke R., 1988, ApJS, 66, 361
Hutchings J. B., Janson T., Neff S. G., 1989, ApJ, 342, 660
Keel W. C., 1980, AJ, 85, 198
Kellermann K. I., Sramek R., Schmidt M., Shaffer D. B., Green R., 1989, AJ, 98, 1195
Kristian J., 1973, ApJ, 179, L61
Lacy M., Rawlings S., Hill G. J., 1992, MNRAS, 258, 828
Lilly S. J., Longair M. S., Allington-Smith J. R., 1985, MNRAS, 215, 37
McCarthy P. J., van Breugel W., Spinrad H., Djorgovski S., 1987, ApJ, 321, L29

MacKenty J. W., 1990, ApJS, 72, 231
MacKenty J. W., Stockton A., 1984, ApJ, 283, 64
McLean I. S., Chuter T. C., McCaughrean M. J., Rayner J. T., 1986, SPIE, 627, 430
Malkan M. A., 1984, ApJ, 287, 555
Malkan M. A., Margon B., Chanan G. A., 1984, ApJ, 280, 66
Meurs E. J. A., Unger S. W., 1991, A&A, 252, 63
Meurs E. J. A., Wilson A. S., 1984, A&A, 136, 206
Miley G. K., Hartsuijker A. P., 1978, A&AS, 34, 129
Miller L., Peacock J. A., Mead A. R. G., 1990, MNRAS, 244, 207
Neff S. G., Brown R. L., 1984, AJ, 89, 195
Neugebauer G., Matthews K., Soifer B. T., Elias J. H., 1985, ApJ, 298, 275
Neugebauer G., Green R. F., Matthews K., Schmidt B. T., Bennet J., 1987, ApJS, 63, 615
Owen F. N., Laing R. A., 1989, MNRAS, 238, 357
Peacock J. A., 1983, MNRAS, 202, 615
Peacock J. A., Miller L., Longair M. S., 1986, MNRAS, 218, 265
Romanishin W., Hintzen P., 1989, ApJ, 341, 41
Romney J. et al., 1984, A&A, 135, 289
Sandage A. R., Freeman K. C., Stokes N. R., 1970, ApJ, 160, 831
Sanders D. B., Scoville N. Z., Soifer B. T., 1988a, ApJ, 335, L1
Sanders D. B., Soifer B. T., Elias J. H., Neugebauer G., Matthews K., 1988b, ApJ, 328, L35
Schlickeiser R., Biermann P. L., Crusius-Wätzel A., 1991, A&A, 247, 283
Schmidt M., 1970, ApJ, 162, 371
Sitko M. L., Zhu Y., 1991, ApJ, 369, 106
Smith E. P., Heckman T. M., 1990, ApJ, 348, 38
Smith E. P., Heckman T. M., Bothun G. D., Romanishin W., Balick B., 1986, ApJ, 306, 64
Sopp H. M., Alexander P., 1991, MNRAS, 251, 14P
Stocke J. T., Liebert J., Gioia I. M., Griffiths R. E., Maccacaro T., Danziger I. J., Kunth D., Lub J., 1983, ApJ, 273, 458
Stockton A., 1982, ApJ, 257, 33
Stockton A., Farnham T., 1991, ApJ, 371, 525
Stockton A., MacKenty J. W., 1987, ApJ, 316, 584
Tadhunter C., Tsvetanov Z., 1989, Nat, 341, 422
Thuan T. X., Puschell J. J., 1989, ApJ, 346, 34
van Breugel W., Miley G., Heckman T., 1984, AJ, 89, 5
Véron-Cetty M. P., Véron M. P., 1991, ESO Scientific Report No. 10
Véron-Cetty M. P., Woltjer L., 1990, A&A, 236, 69
Yee H. K. C., 1987, AJ, 94, 1462